



Review

State-of-the-art in heat exchanger additive manufacturing



Inderjot Kaur, Prashant Singh*

Department of Mechanical Engineering, Mississippi State University, MS 39762, USA

ARTICLE INFO

Article history:

Received 9 February 2021

Revised 4 June 2021

Accepted 14 June 2021

Available online 28 June 2021

Keywords:

Heat exchangers

Additive manufacturing

Heat transfer enhancement

ABSTRACT

The progress in additive manufacturing (AM) sector has transformed the ways in which heat exchangers (HXs) can be fabricated. The complex and freeform designs which could not be realized by conventional manufacturing routes can now be realized through AM technologies. The weight, volume, load bearing capabilities and manufacturing cost reductions are some of the other benefits that AM can provide over the conventional manufacturing. The relative benefits of using AM to make heat exchangers, however, are accompanied by various inherent challenges related to the process parameters, surface quality and material choice. A comprehensive understanding of the fabricated HX surface quality is imperative to explain the resulting flow and thermal characteristics. This study focuses on analyzing the thermal-hydraulic performance of additively manufactured HXs such as rough surfaces, microchannels, surface area and turbulence promoters, cellular materials, heat pipes, turbomachinery cooling designs, and jet impingement cooling concepts. The review of the existing literature suggests that the inherent surface roughness is the key consideration across different types of heat exchanger configurations manufactured by metal additive manufacturing. Significant deviation of the manufactured dimensions is observed relative to the intended design, especially when the dimensions approach the manufacturing limits. With the continuously improving AM technologies in terms of final product surface quality, dimensional accuracy, and realization of smaller length scales with accuracy, one can expect exciting times ahead in heat exchanger development and to this end, the review paper may serve as an essential reference tool.

© 2021 Elsevier Ltd. All rights reserved.

1. Introduction

The progress in additive manufacturing (AM) technologies in the past three decades has significantly influenced the heat exchanger (HX) design and development. There is continuous effort to design efficient and compact heat exchangers which are lightweight and require less material volume. Multifunctional HXs have many applications where both heat dissipation and load bearing capabilities are desirable. Recent studies in AM and thermal management sector have focused on depicting the potential of AM in producing such next-generation HXs.

The HXs are widely used in aerospace industry, food industry, turbine technologies, chemical processing factories, automobiles, electronic devices and data centers, nuclear plants, solar receivers, waste-heat recovery systems, air-conditioning units in buildings, etc. The employment of the heat exchanging devices, therefore, span from miniature micro-electronic chips to large-scale buildings. The traditional HX studies could be categorized in two broad senses, one that aims at the development of integrated structures

such as cross-flow and parallel-flow heat exchangers, microchannel circuits, etc. and the other focuses on the analysis of individual heat transfer enhancement features such as pin-fins, dimples, ribs, protrusions, metal-foam inserts, helical/twisted tape inserts, vortex generators, etc. [1–7]. The integrated structures are typically stand-alone devices which promote the heat transfer primarily due to their architectural design or dimensional scales. For example, shell-tube type arrangement promotes interaction between the two heat exchanging fluids where one fluid flows through tubes and other through the surrounding shell [8]. On the other hand, heat transfer enhancing feature could be introduced in the basic machinery or already tailored HX to further augment the performance, for example, ribs and pin-fins are introduced in the cooling channels of the turbine blades to augment the cooling and promote structural integrity. The efficiency of plate-fin heat exchangers is enhanced further by introducing the winglets on the plate surfaces [9].

Conventional technologies for manufacturing HXs include milling, shearing, drilling, casting, and forming. The assembly of different parts is generally achieved by welding or brazing. These traditional technologies are generally 'subtractive' in nature because they are based on the removal of excess material to obtain the desired geometry, an operation which by nature results in wastage of material. Moreover, the HXs assembled from dif-

* Corresponding author at: 479-1 Hardy Rd, 217 Carpenter Hall, Mississippi State, MS 39762, USA

E-mail address: singh@me.msstate.edu (P. Singh).

Abbreviations

AM	Additive manufacturing
CAD	Computer-aided design
CFD	Computational fluid dynamics
CGDS	Cold gas dynamic spraying
CNC	Computer numerical control
COP	Coefficient of performance
d_h	Hydraulic diameter
DMLS	Direct metal laser sintering
EBM	Electron beam melting
EDM	Electrical discharge machining
f	Friction-factor
h	Heat transfer coefficient
HP	Heat pipe
HX	Heat exchanger
k	Thermal conductivity of fluid
K	Permeability
L	Length across which pressure drop is measured
LED	Light emitting diode
m	Mass of heat exchanger
M	Blowing ratio
MC	Microchannel
MJ	Microjet
MMC	Manifold-microchannel
MPBMC	Multi-pass branching-microchannel
Nu	Nusselt number
ΔP	Pressure drop
PMMC	Permeable membrane-microchannel
Q	Heat duty of heat exchanger
r	Pore radius
R_a	Average roughness
Re	Reynolds number
SLA	Stereolithography
SLM	Selective laser melting
T	Temperature
TBC	Thermal barrier coating
TPMS	Triply periodic minimal surfaces
ΔT	Temperature difference
U	Velocity
VDF	Volumetric distance fields
WMC	Wavy-microchannel
z_i	Roughness height
<i>Greek symbols</i>	
ν	Kinematic viscosity
μ	Mean surface height
η	Efficiency, effectiveness (based on context)
ρ	Density of the working fluid
ϵ	Absolute pipe roughness
<i>Subscripts</i>	
∞	Mainstream
aw	Adiabatic
c	Coolant
eff	Effective
s	Solid

ferent parts may be susceptible to working fluid leakage if flow-tight connections are not achieved. It is complicated to manufacture complex designs via conventional means because of the limited machining possibilities through "subtractive" procedures. The realization of these complex forms at very small scales becomes even more challenging. Despite the challenges posed by conven-

tional manufacturing methods, these technologies are used till date to successfully fabricate HXs for various applications.

Additive manufacturing technologies gained popularity as they provide freedom in design of complex elements in HXs, help achieve small length scales with acceptable accuracy, and overcome many other shortcomings of the conventional technologies. AM processes build a part through layer-by-layer addition of the material which results in minimal material wastage. Programming-controlled environment makes the realization of complex computer-aided designs (CAD) possible. Moreover, the entire part can be manufactured in one monolithic build which eliminates the need to generate the individual components separately and thus prevents leakage issues, if any. The HXs involving the use of inserts of some sort can be directly printed on the substrate being actively cooled resulting in good interface connections for heat conduction as opposed to conventional brazing.

The freedom of conceptualizing and making complex designs through AM technologies has its own inherent challenges. Process parameter optimization, surface-roughness control, support-structure removal, post-processing requirements, compatible raw materials, and cost-competitiveness with respect to conventional methods for bulk production are active areas of discussion. Despite the challenges, AM technologies can successfully make HXs in metals, polymers, and ceramics. Klein et al. [10] recently reviewed the progress in additive manufacturing of HXs derived from metal, polymer and ceramic materials and discussed the cost-competitiveness of the AM methods. Deisenroth et al. [11] provided comprehensive review on polymer and polymer composite-based HXs where the details of different AM techniques, polymer materials and challenges in manufacturing were presented. Nafis et al. [12] reviewed additively manufactured heat sinks for electronic cooling application and highlighted the achievements and limitations of additive manufacturing. The potential of Selective Laser Sintering technology was thoroughly reviewed by Jafari and Wits [13], where the authors provided an overview of the different HX investigations that exist in the literature and highlighted the need to specify standards for property assessment of additively manufactured HXs.

In the present study, an overview of the additively manufactured HXs is provided by categorizing them into seven main sections: surface roughness, microchannels, area and turbulence promoters, cellular materials, heat pipes, turbomachinery, and jet impingement. Detailed description of the performance of these HXs is provided with critical comparison with the conventional HXs wherever possible. Unlike most of the reviews mentioned above, this study evaluates the additively manufactured HXs primarily from flow and thermal transport perspective rather than material and process considerations. Also, the manufacturability and thermal-hydraulic performance of bio-inspired cellular structures and turbomachinery cooling concepts manufactured via AM technologies is discussed here which has not been presented in the aforementioned reviews. The inherent challenges in additive manufacturing and future opportunities are also highlighted in the end.

2. Additively manufactured HXs

This section presents detailed discussion on additively manufactured HXs which are categorized as shown in Fig. 1.

2.1. Surface roughness

Surface roughness is mostly a desirable feature for promoting heat transfer from a surface, especially when these roughness scales are large enough to disrupt the near-wall viscous layer in turbulent flows. Artificial roughness can be introduced on the

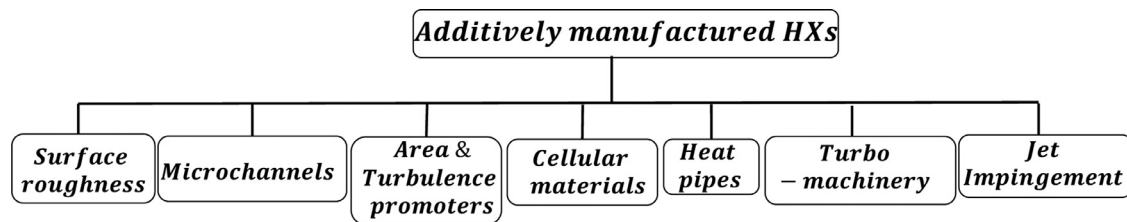


Fig. 1. Categorization of additively manufactured HXs

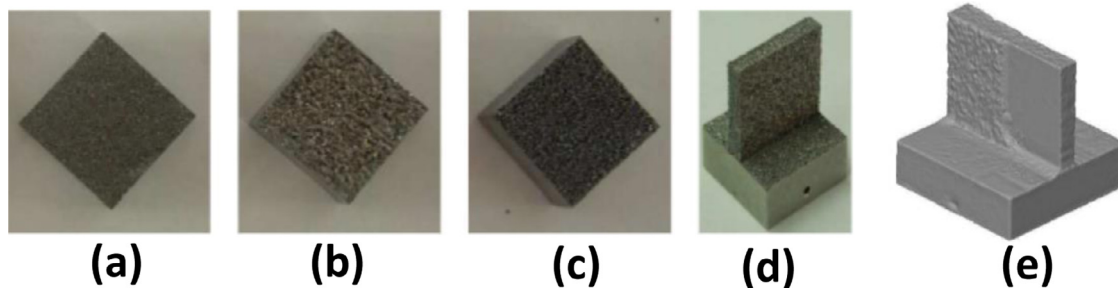


Fig. 2. Samples with average roughness a) $R_a = 16 \mu\text{m}$, b) $R_a = 24 \mu\text{m}$, c) $R_a = 43 \mu\text{m}$, d) fin-surface with $R_a = 22 \mu\text{m}$, e) sample d smoothed by milling [14].

walls interacting with working fluids by mounting some turbulence promoting features, but this section focusses on roughness generated on the surfaces while manufacturing. Powder bed fusion technologies such as Selective Laser Melting (SLM) and Direct Metal Laser Sintering (DMLS) are a sub-class of AM processes which melts or sinters the powdered material layer-by-layer to create three-dimensional solid structure. The final product exhibits surface roughness which is influenced by process parameters and build orientation, and metered roughness can be beneficial for heat transfer enhancement applications.

Ventola et al. [14] reported convective heat transfer coefficient enhancement over three horizontal plates and one orthogonal fin prepared by DMLS in AlSi10Mg material with four different average roughness levels (R_a), as shown in Fig. 2(a-d). Sample with the highest roughness parameter provided maximum heat transfer enhancement of about 73% and average of ~63% over the investigated Reynolds number range with respect to smooth surface prepared by milling ($R_a = 1 \mu\text{m}$). The fin geometry also showed significant enhancement but for complete analysis, the part was later smoothed on horizontal plate and half of the fin surface (Fig. 2e) by milling operation. The heat transfer enhancement was higher when smoother surface was near the leading edge.

Stimpson et al. [15,16] investigated the effect of surface roughness on the heat transfer and pressure drop characteristics of eleven coupons having rectangular micro- and mini- channels printed in cobalt-chrome-molybdenum superalloy (CoCr) and Inconel 718 via DMLS. The roughness of these coupons varied between $R_a = 9.6 \mu\text{m}$ to $13.3 \mu\text{m}$ which was apparent in the CT scan images of the printed samples. When compared with reference smooth coupon having round channels manufactured via conventional machining, 55% reduction in heat transfer rate was achieved for 70% decrease in mass flow rate at fixed pressure drop conditions. The authors also presented correlations for predicting friction factor and Nusselt number variation in rough channels produced by AM technologies.

Heat transfer enhancement due to surface roughness comes at the cost of increased pressure drop. The protruded roughness in small-scale channels can alter the effective hydraulic diameter, mass flow rate estimations and transition Reynolds number as well. The protruded roughness can become detrimental in cases where its scales are large enough to block the channels or pores of the designed geometry. Therefore, proper characterization of sur-

face properties post manufacturing and optimization of the process parameters to gain acceptable roughness is needed.

Snyder et al. [17] investigated the effect of build direction on the quality of internal features of minichannels additively manufactured via DMLS in Inconel 718. Consequently, its impact on the thermal-hydraulic performance due to resultant surface roughness and tolerance was analyzed. Three different shapes, namely, cylindrical, diamond and teardrop were manufactured with horizontal built orientation. No support structures were generated within the channels because of the difficulty in their removal post printing, due to which the upper edges of the diamond and teardrop shapes collapsed. All the manufactured samples had different average surface roughness, transition Reynolds number and friction factor values but similar Nusselt number. It should be noted that the end-product channels were not diamond or teardrop shaped in their true sense. This study highlights the challenges for AM technologies in producing small-scale channels of different shapes with intended surface finish and shapes. Building high quality parts require support structures sometimes, the removal of which needs post-processing arrangements, and this could either be very cost-intensive for complex and small scale parts or almost impossible by cheap but time-consuming manual means.

The characterization of surface roughness through process parameter optimization is reported by several authors [18–22] for different powder bed fusion AM technologies. While the discussion until now has primarily focused on the metal AM technologies only, there are attempts to investigate the surface quality of polymer and ceramic-based additively manufactured parts [23,24] as well but these studies do not focus on investigating the effect of the roughness on the thermal transport. The studies [14,15,17] are prominent investigations on the concerned topic and exhibit the possibility of exploring the benefits of inherently generated surface irregularities via additive manufacturing in both external and internal flow scenarios. The implications of surface roughness on the performance of HXs are many, which are discussed in detail in the subsequent sections.

2.2. Microchannels

The development of miniaturized electronic equipment drives the need to develop complementary small-scale heat sinks which can dissipate very high heat fluxes to ensure prolonged life of

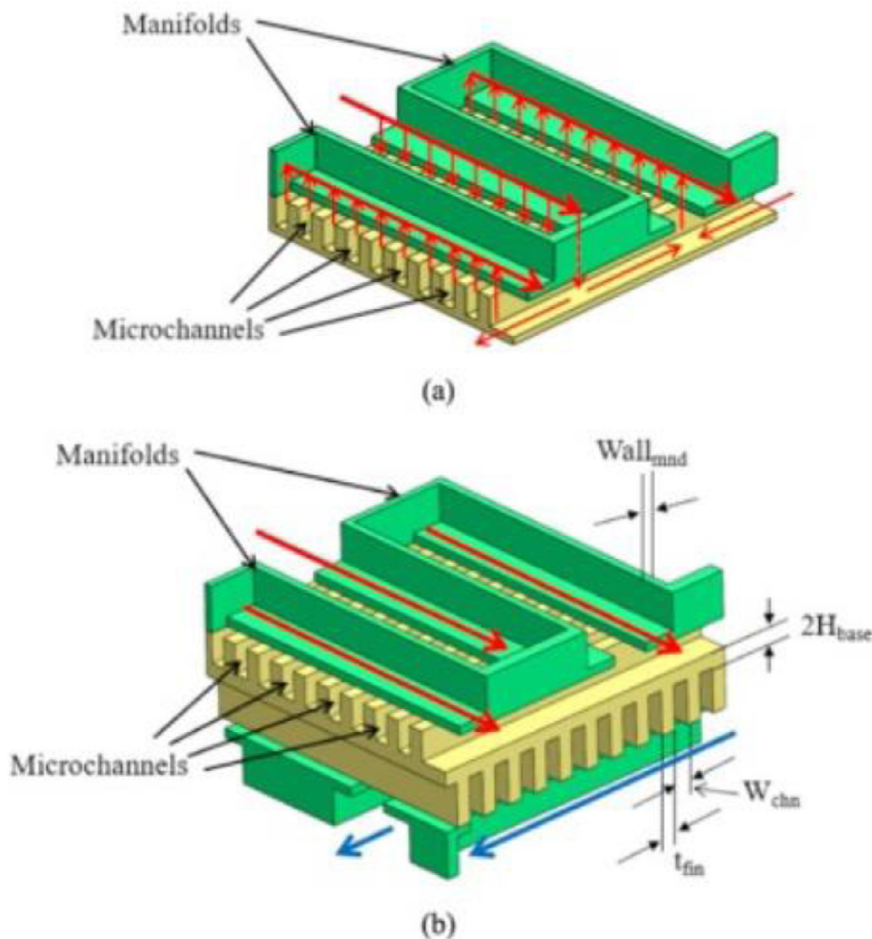


Fig. 3. (a) Manifold-microchannel HX [31]. With permission to reuse from Elsevier.

the systems. Prior investigations on microchannels have demonstrated their ability to dissipate high power densities [25,26]. In conventional microchannel heat sinks, small hydraulic diameter conduits ($10 \mu\text{m} < d_h < 200 \mu\text{m}$ for microchannels and $200 \mu\text{m} < d_h < 3 \text{ mm}$ for minichannels as per Kandlikar and Grande [27]) run parallel to the heated base and the fluid flowing in these channels are the heat carriers. Some of the conventional techniques for the manufacturing of microchannels include wafer dicing, micro-electro discharge machining, ultrasonic and waterjet machining, laser-machining, wet chemical etching, and deep reactive ion-etching. The separately manufactured parts are often joined together by fusion bonding, anodic bonding, or adhesive bonding [27].

Microchannel heat exchangers are typically characterized by large pressure drops which can be caused by flow maldistribution in channels and long streamwise flow lengths. Manifold-microchannel heat exchangers are suggested as alternatives to the conventional microchannel heat exchangers, where a manifold structure is placed on the top of the parallel running microchannels as shown in Fig. 3. This manifold structure resting on the top of microchannels distributes the coolant fluid through multiple inlet and outlet ports. The flow length in this configuration is reduced which improves the hydraulic characteristics of the heat exchanger.

Traditionally, the manifolds and microchannels are manufactured separately and then joined together by one of the bonding techniques mentioned above, a process which can increase the lead time and can affect the performance if not conducted properly. Ad-

ditive manufacturing technology can build the manifold and microchannels as a single part to ensure proper interface between the two components. More complex and optimized designs for the channels can also be realized by AM which might be very challenging, if not impossible, by the traditional techniques.

Arie et al. [28] employed multi-objective optimization technique to maximize coefficient of performance (COP, defined as the ratio of heat duty to pumping power) and gravimetric heat transfer density ($Q/m\Delta T$, where Q is the heat duty and m is the mass of HX) of a manifold-microchannel. The optimization was performed on five samples with different fin- and manifold-thicknesses printed in stainless steel via DMLS. Reduction of fin-thickness from $150 \mu\text{m}$ to $50 \mu\text{m}$ and manifold-thickness from $300 \mu\text{m}$ to $150 \mu\text{m}$ increased gravimetric heat transfer density by 20–40% and 10–30%, respectively, at same $COP/\Delta T$. Since $150 \mu\text{m}$ and $300 \mu\text{m}$ dimensions for fin and manifold, respectively, were below the current recommended safe manufacturing limit of DMLS, the authors concluded that manifold-microchannel HX performance can be significantly improved if smaller limits are reached in the future. The optimized manifold geometry provided up to ~60% increment in gravimetric heat transfer density as compared to conventional wavy-fin surface. This implies that removal of same heat load to maintain a given temperature difference could be achieved by using manifold-microchannel having significant lesser weight than wavy-fin surface.

In another study, Arie et al. [29] manufactured air-to-water manifold-microchannel HX in titanium alloy (Ti64) via DMLS with the fins inclined at 45° . The manufactured fin-thickness was ~0.25

mm as opposed to intended ~0.15 mm but no clogging of the channels was observed during inspection. The manifold channels in this study were tapered to adjust the flow and pressure as opposed to straight manifolds in [28]. Air-side heat transfer coefficient of ~180 W/m²K was reported for pressure drop of ~ 100 Pa for investigated range of air-side Reynolds number of < 100. The heat transfer coefficient provided by manifold-microchannel was higher than conventional wavy, plain-plate, and louvered fin for same pressure drop. Similar air-to-water tapered-manifold microchannel heat sink design for dry cooling applications in power plants was investigated by Arie et al. [30]. The manifold-microchannels were manufactured in stainless steel (SS17-4), titanium alloy (Ti64) and aluminum alloy (AlSi10Mg) via DMLS. About 20% deviation in the fin- and microchannel width sizes was observed between the manufactured and intended CAD designs. Also, partial clogging of channels was present due to residual powder. These dimensional inaccuracies were reported to be more prominent in stainless-steel sample as compared to titanium alloy. Pressure drop for the investigated air-side Reynolds number of up to ~400 was 50-2,000 Pa for Ti64 and 200-7,000 Pa for SS17-4 and AlSi10Mg. The air-side heat transfer coefficient was 100-450 W/m²K, 100-600 W/m²K, and 100-900 W/m²K for Ti64, SS17-4, and AlSi10Mg, respectively. The differences in the heat transfer coefficient and pressure drop parameters for the three samples having similar geometry and intended dimensions was attributed to the inaccuracies that occurred while manufacturing. Microchannel heat sink with tapered manifold manufactured in Inconel 718 via DMLS was investigated by Zhang et al. [31] for high temperature applications with nitrogen on the hot-side and air on the cold-side. About 25% enhancement in heat transfer density (ratio of heat duty and mass) was reported at COP of 62 relative to conventional plate-fin heat exchangers.

Collins et al. [32] compared the thermal and hydraulic performance of manifold-microchannel with conventional straight microchannels, both additively manufactured in AlSi10Mg via DMLS. The manifold design provided lower pressure drop values, but higher thermal resistance as compared to straight microchannel heat sink, contrary to what was expected. The authors argued that the higher thermal resistance (K/W) of the manifold design was due to smaller convective area available and suggested that narrower channels (higher aspect ratio) should be used to enhance the performance of manifold-microchannels. The experimental pressure drop data of straight channel showed good agreement with existing correlations in laminar regime but showed early transition due to surface roughness, a phenomenon typically observed in samples prepared by metal AM technologies.

The channel shapes can be modified and optimized to enhance the thermal-hydraulic performance of the microchannels. Kirsch and Thole [33-35] performed extensive numerical and experimental investigation to characterize the performance of wavy microchannels. The authors investigated the prospective use of additively manufactured wavy microchannels in cooling gas turbine components. Coupons made with wavy channels in Inconel 718 via DMLS were tested for different wavelengths. About 50% heat transfer enhancement was obtained with respect to straight channels for low Reynolds number range (< 4,000), and it was found that flow structures were dominant mechanism at lower Reynolds number contrary to surface roughness at higher Reynolds numbers. The authors further obtained numerically optimized microchannels and communicating microchannels.

AM technologies have opened space to manufacture user-defined complex forms but the studies showing the potential of combining the numerical optimization techniques with AM are very rare. It is possible that the geometry optimized to achieve a certain objective might be complex to be successfully manufactured by traditional methods. With the current capabilities of com-

putational fluid dynamics (CFD) and AM, the collaboration of both can give highly efficient HXs with desired qualities.

The inevitable occurrence of roughness on the surfaces printed via AM technologies has been briefly discussed in the Section 2.1. Different roughness profiles can be realized on printed parts when a given design is printed either in different materials using same technology or in same material via different manufacturing technologies. Kirsch and Thole [36] manufactured an optimized microchannel heat exchanger in resin via Stereolithography (SLA) and in metal via DMLS to study the effect of surface roughness and wall shapes (design) on the performance of HX. The parts manufactured by SLA were smoother and the experimental results were close to the computational predictions. On the other hand, the metal samples provided significant deviation especially in the friction factor, which was dependent on the surface roughness. DMLS is currently the most commonly used technique for manufacturing microchannels in metal and the fin thickness dimensions of ~0.15 mm are the current manufacturing limits of this technique. An effort to test the limits of the metal AM and further push it to smaller length-scales appears promising.

Collins et al. [37] proposed a novel microchannel composed of porous walls in order to enhance the thermal performance and reduce pressure drop as compared to manifold-microchannel heat sink. Since fabricating microchannels with porous membranes is difficult by existing traditional methods, AM can be used to generate such complex features. A porous membrane of intended thickness of 400 μm at porosity ~ 23% was generated which on micro-imaging showed effective thickness of only 300 μm . DMLS primarily sinters the powdered metal together to create layers while printing. The process parameters can be tuned to control the porosity of the final structure. The investigated porous-membrane microchannel showed 17% and 28% reduction in thermal resistance and pressure drop, respectively, at constant pumping power of 0.018W as compared to manifold-microchannels. The authors also proposed a reduced order model to predict the pressure drop and thermal resistance of the porous membrane sample which significantly deviated from the experimental results. The difference in results was attributed to reduced nature of the model, surface roughness characteristics, and imprecise thermal conductivity of aluminum. It is worth noting that difference in the predicted and obtained Nusselt number values by Collins et al. [32] was also attributed to uncertainty in the nominal thermal conductivity value. The material properties, such as thermal conductivity, in additively manufactured HXs are not known with high certainty due to which the thermal performance of these HXs cannot be predicted properly. A thorough characterization of the thermo-physical properties of the materials is, therefore, important for obtaining accurate results.

The study on porous membrane is significant to identify the superiority of permeable membranes in microchannels. Although it is challenging for AM technologies at the moment, but future advancements can allow more control over customizing the walls as well. A study by Kaur and Singh [38] showed that even a single-cell thick wall of strut-based cellular topologies can yield in significant heat transfer. Therefore, user-defined complex topologies can be used as separating membranes in micro-heat exchangers.

Some studies have focused on enhancing the performance of manifold-microchannels by introducing turbulence promoting features such as pin-fins in the manifold path. Alsulami et al. [39] tried to enhance the thermal performance of the manifold microchannels by introducing the pins in the flow path and changing orientation of channels manufactured via selective laser melting (SLM). The modified configurations were not capable of providing enhanced performance relative to the traditional baseline manifold-microchannel heat sink, thereby, suggesting that adding more complexity does not necessarily improve the performance.

The flow physics in the channels significantly govern the heat transfer from a surface. Therefore, any novel design should aim at modifying the flow field positively to improve the performance which is not directly related to level of complexity but how a complexity affects the flow.

Yameen et al. [40], Tiwari et al. [41], and Keramati et al. [42] manufactured the manifold-microchannels and evaluated their performance. Panse and Ekkad [43] investigated the thermal and hydraulic performance of additively manufactured single- and two-pass inline-straight, staggered-straight, oblique-fin, and trapezoidal fin microchannels. Oblique fin and trapezoidal fin microchannels yielded the least thermal resistance for a given pressure drop amongst all the configurations.

Joshi et al. [44] compared the thermal and hydraulic properties of conventionally machined diffusion-bonded aluminum multi-pass branching microchannel with additively manufactured same heat sink. The heat transfer and pressure drop in additively manufactured part was higher than machined part due to surface roughness. The surface roughness on the additively manufactured part was reported to be an order-of-magnitude higher than machined part. This study provided a direct comparison of additively manufactured and conventionally made part quality establishing that as far as traditional geometries or design forms are concerned, conventional manufacturing routes can still provide high surface quality part and expected results. The surface non-uniformity influences the results so much that the validity of already established correlations which were derived after testing the traditionally manufactured parts becomes difficult for additively manufactured heat sinks. Although, some experimental studies have shown good agreement with the microchannel correlations in laminar region, the transitional limits are, however, very different.

Table 1 shows the typical dimensions encountered in additively manufactured micro- and mini-channels. The deviations in manufactured (actual) and intended (CAD) dimensions are also reported. The average surface roughness (R_a) is defined as following [16]:

$$R_a = \frac{1}{n} \sum_{i=1}^n |z_i - \mu| \quad (1)$$

z_i is the roughness height at a given point and μ is the mean surface height.

Surface roughness of about $\sim 9.5 - 20 \mu\text{m}$ could be observed with deviation of about $\sim 12\%$ in actual and intended hydraulic diameter. The roughness characteristics and deviations in the manufactured and CAD designs are different when same geometry is printed with different materials.

Fig. 4a shows the friction factor ($2\Delta Pd_h/L\rho U^2$) and **Fig. 4b** shows the Nusselt number (hd_h/k) as a function of Reynolds number for rough mini- and micro-channels. Hydraulic and thermal characteristics of minichannels containing winglets are also plotted as reported by Rastan et al. [45]. 1x refers to baseline coupon and 2x refers to the scaled-up version of the same geometry. Co and In are the materials, Cobalt and Nickel alloys, respectively and the numbers 1 and 2 succeeding the material specification denotes two different dimensions for same material. The smooth channel data prepared via conventional processes showed good agreement with the plain-channel correlations with relatively higher flow losses at $Re \sim 700-2,000$ due to the entrance effects. The additively manufactured channels with roughness showed significant deviation in both laminar as well turbulent regimes. The transition to turbulent regime for additively manufactured channels occurred at Reynolds number lower than that for smooth channel. Same geometry printed in different material also showed varying flow loss property due to different surface roughness as observed in **Table 1**. The Nusselt number is also augmented relatively to smooth channel in rough micro- and mini- channels for different

channel shapes (**Fig. 4b**). Minichannels with rectangular winglet structures shows the maximum heat transfer in the laminar range but at the cost of significantly higher pressure drop.

Pressure drop characteristics of channels with varying surface roughness have been investigated by several authors in the past [46,47]. Friction factor ($2\Delta Pd_h/L\rho U^2$) is a non-dimensional parameter derived using the pressure drop gradient ($\Delta P/L$), characteristics length scale/hydraulic-diameter (d_h), fluid density (ρ), and flow velocity (U). For a given geometry and working fluid, the friction factor is a function of the Reynolds number for smooth channels. However, with the introduction of roughness, the friction factor becomes a function of both, the Reynolds number and the relative roughness (ϵ/d_h , absolute pipe roughness-to-channel hydraulic diameter ratio). Classic Moody chart shows the variation of friction factor with respect to flow Reynolds number for $\epsilon/d_h \leq 5\%$. The friction factor reduces with increasing Reynolds number following the relationship $fRe = 64$ in the laminar region. In classic Moody chart, the relative roughness up to 5% has no influence on the friction factor in laminar region. However, in rough pipes the friction factor shows no dependence on the Reynolds number but becomes a function of relative surface roughness in the fully turbulent flow regime. Huang et al. [46] experimentally determined the effect of surface roughness on friction factor in macro tubes ($d_h=19 \text{ mm}$) in the laminar flow regime. For relative roughness greater than 5%, the obtained data showed significant deviations from the standard correlation and yielded values of fRe greater than 64. In **Fig. 4a**, the additively manufactured coupons showed significant deviation from $fRe = 64$ trendline in laminar regime and appear to reach an asymptotic value at fully turbulent conditions. Dai et al. [48] investigated the effect of surface roughness on liquid friction and transition in micro- and mini- channels. No significant effect was observed for relative roughness $\leq 1\%$ on the friction factor as well as transition Reynolds number. The relative roughness $> 1\%$ and $> 5\%$ was recommended as threshold for considering roughness effects in micro/minи- and macro- channels, respectively. The critical Reynolds number at which the transition from laminar to turbulent regime occurs is also significantly influenced by the relative roughness of the channel along with the magnitudes of friction factor as discussed above. General accepted value of this transition Reynolds number is around ~ 2300 for smooth surfaces, but early transitions have been observed in literature for surfaces characterized by high relative roughness. Early transition in rough microchannels was reported by Kandlikar et al. [47], where the transition occurred at critical Reynolds number of ~ 800 and 350, for relative roughness of 0.06 and 0.14, respectively. The coupons in **Fig. 4a** showed a wide range of Reynolds number at which the transition occurred from laminar to turbulent regime. The difference is attributed to different relative roughness values encountered in different coupons, only if the other manufacturing process deviations are ignored.

The heat transfer augmentation is plotted against the corresponding enhancement of pressure drop in **Fig. 5**. **Fig. 5a** is reproduced with the adjusted friction-factor range (x-axis) in **Fig. 5b** for clear data representation. The performance of the additively manufactured coupons is made with some common heat exchange enhancement technologies that exist in the literature such as rib-turbulators, dimples, pins-fins, and grooves. The solid-colored markers represent additively manufactured samples whereas hollow markers are for conventionally made configurations. The rectangular, teardrop, diamond and wavy- channels manufactured via AM technologies have similar heat transfer and pressure loss characteristics to many rib-turbulator configurations. Rectangular, teardrop, and diamond channels show small change in Nusselt number values over a wide friction factor augmentation range. Significantly higher pressure drops observed in printed coupons signifies the need to further characterize the surface roughness in de-

Table 1

Dimensions of additively manufactured micro- and mini-channels. Also shown is the deviation of these relative to intended design

Reference & Geometry	Process	Material	Fin-thickness, t_{fin} , mm		Manifold-thickness, t_{mnd} , mm		Channel width, W , mm		Channel Height, H , mm		Hydraulic Diameter, d_h , mm		Average surface roughness, R_a , μm	Relative roughness, R_a/d_h	Percentage Deviation from intended design			
			CAD	Actual	CAD	Actual	CAD	Actual	CAD	Actual	CAD	Actual			t_f	H	W	d_h
Stimpson et al.[15]	DMLS	CoCr	0.38				0.457	0.450	1.016	1.028	0.631	0.626	9.6	0.015	1.18	-1.53	-0.79	
Stimpson et al.[15]	DMLS	CoCr	0.38				0.914	0.898	2.032	2.036	1.261	1.246	12.3	0.010	0.19	-1.75	-1.18	
Stimpson et al.[15]	DMLS	CoCr	0.55				0.305	0.296	0.660	0.694	0.417	0.415	10.3	0.025	5.15	-2.95	-0.47	
Stimpson et al.[15]	DMLS	CoCr	0.68				0.610	0.516	1.321	1.302	0.834	0.739	12.7	0.017	-1.44	-15.41	-11.39	
Stimpson et al.[15]	DMLS	CoCr	0.68				0.610	0.601	0.610	0.626	0.610	0.614	9.5	0.015	2.62	-1.47	0.655	
Stimpson et al.[15]	DMLS	Inconel 718	0.38				0.457	0.453	1.016	1.047	0.631	0.632	10.5	0.017	3.05	-0.87	0.16	
Stimpson et al.[15]	DMLS	Inconel 718	0.38				0.914	0.919	2.032	2.083	1.261	1.275	10.9	0.009	2.51	0.55	1.11	
Stimpson et al.[15]	DMLS	Inconel 718	0.55				0.305	0.355	0.660	0.690	0.417	0.469	11.9	0.025	4.54	16.39	12.47	
Stimpson et al.[15]	DMLS	Inconel 718	0.68				0.610	0.683	1.321	1.406	0.834	0.920	13.8	0.015	6.43	11.96	10.31	
Stimpson et al.[15]	DMLS	Inconel 718	0.68				0.610	0.660	0.610	0.669	0.610	0.664	13.3	0.020	9.67	8.19	8.85	
Snyder et al. [17]	DMLS	Inconel 718									0.508	0.569	16.1	0.028				
Snyder et al.[17], teardrop-shaped channel	DMLS	Inconel 718									0.508	0.599	13.5	0.022				
Arie et al. [28], MMC	DMLS	SS	0.05-0.3		0.3-0.7		0.05-0.25		0.2-5									
Arie et al.[30], MMC	DMLS	SS, aluminum alloy	0.15	0.235			0.27	0.185	1.2									
Zhang et al. [31], MMC	DMLS	Inconel 718	0.165		0.5		0.340								13.4	-4.2		
Collins et al. [32], MMC	DMLS	Aluminum alloy	0.5		1.5		0.5		0.5		0.5		20					
Kirsch et al.[33], WMC	DMLS	Inconel 718	0.5						1		0.68	0.61-0.65		0.011-0.026				
Kirsch et al.[35], WMC	DMLS	Inconel 718							1		0.58-0.55	0.64-0.6		0.018-0.015				
Collins et al. [37], PMMC	DMLS	Aluminum alloy	0.4	0.3					2									
Alsulami et al. [39], MMC	SLM	SS	0.48				0.48		1		0.64							
Keramati et al. [42], MC	DMLS	Maraging steel	0.10, 0.125, 0.150	0.133, 0.156, 0.188														
Joshi et al. [44], MPBMC		Aluminum alloy											12					

*MMC - manifold-microchannel; WMC - wavy-microchannel; PMMC – permeable membrane-microchannel ;MPBMC – multi-pass branching-microchannel

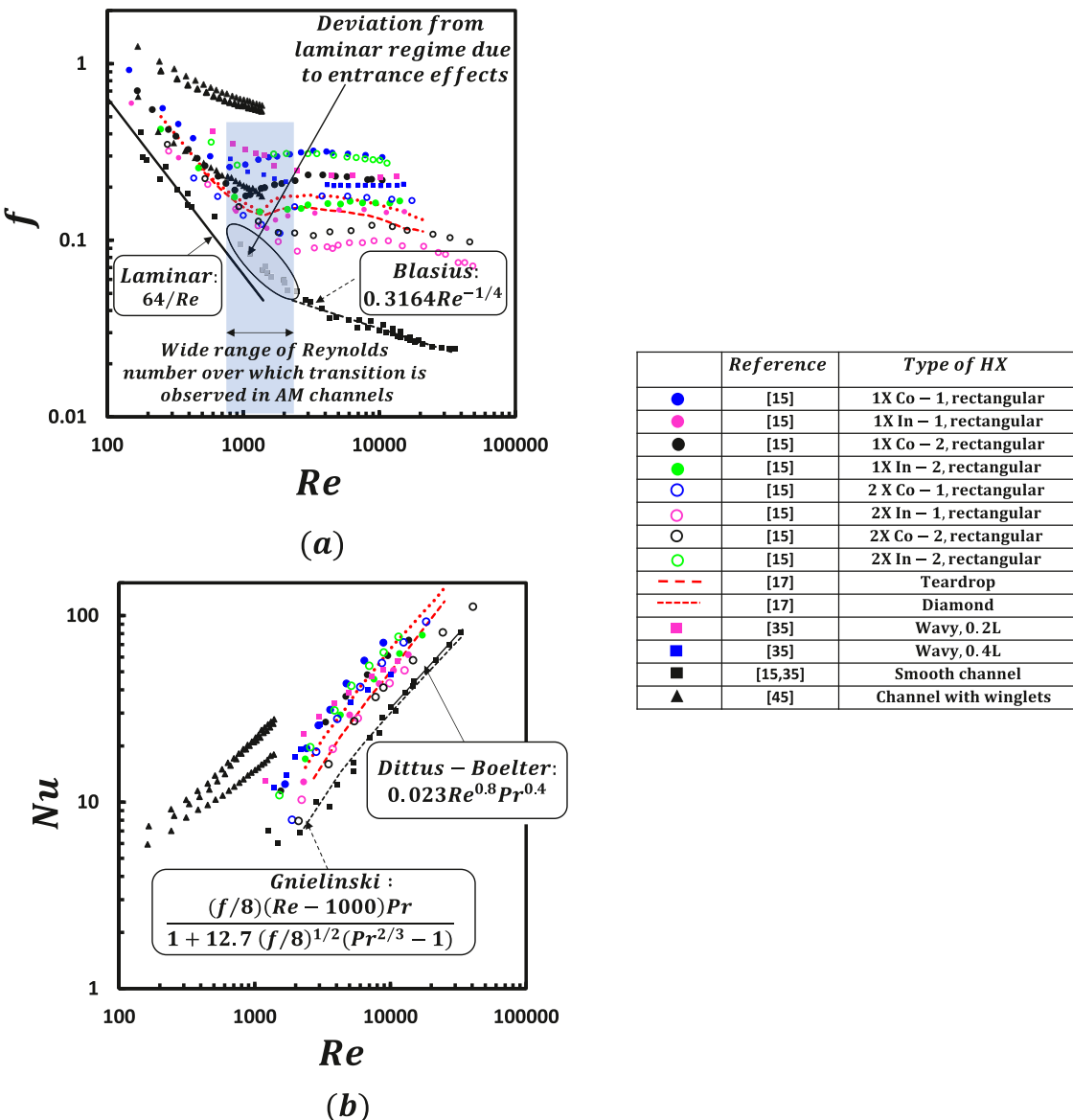


Fig. 4. (a) Friction factor and (b) Nusselt number as a function of channel Reynolds number for mini- and micro-channels (figure reconstructed from above references)

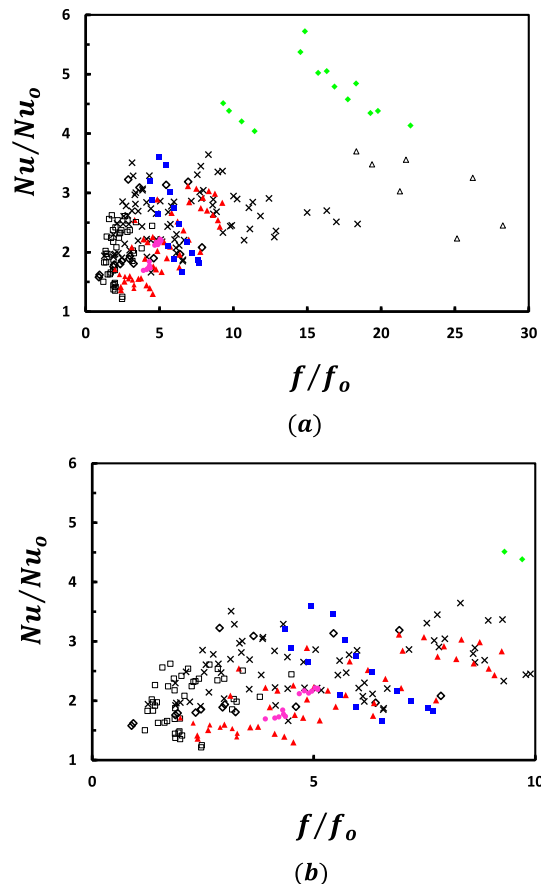
tail and analyze the achievable mass flow reductions relative to smooth channels at fixed pressure drop conditions while incurring acceptable reduction in the heat transfer. The slope of heat transfer enhancement trends in wavy-microchannels is larger than other channels.

2.3. Area and turbulence promoters

One of the fundamental ways to augment net heat transfer from a surface is to either increase the wetted surface area or promote turbulence and fluid mixing, for which many cooling technologies have already been extensively investigated. Comprehensive comparison of various passive heat transfer augmentation technologies such as pin-fins, dimples and rib-turbulators was provided by Ligrani et al.[58]. While different shapes and dimensions for these features could be successfully generated by traditional manufacturing methods, AM can be beneficial for three major reasons, a) to make complex customized shapes which are beyond the tooling capabilities of traditional methods to carve out, b) achieving micro-scale dimensions for these features to be used in micro-HXs such

as microchannels discussed above, and c) elimination of the bonding process as the feature can be directly printed on the substrate.

Kirsch and Thole [57] studied cylindrical pin-fins in a microchannel manufactured in Inconel 718 powder via DMLS for different spanwise and streamwise spacings. The surface roughness and deviations in pin shape from circular profile increased with increasing pin-fin density. Fig. 6a shows the CT scan image in which the surface roughness was apparent on both the endwalls and pin-fin surfaces. When compared to the smooth traditionally built low-aspect ratio pin-fin arrays from literature, the gain in pressure drop of additively manufactured samples surpassed the achieved heat transfer augmentation due to roughness. The comparison of heat transfer gain relative to that in pressure drop amongst the four additively manufactured samples showed that the pin-spacing had little influence on heat transfer but significantly impacted the pressure drop. Thus, a wider spacing (a smaller number of pins) could be used to save the material and cost of production to obtain similar thermal performance. Since the comparison in this investigation was made with similar traditionally built geometry, this study did not indicate any value added by AM from design perspective



X - Rib turbulators [6,49,50], □ - dimples [51–54], ◇ - angled groove [55], △ - pin fins [56], ▲ - rectangular minichannels [15], ● - teardrop and diamond minichannels [17], ■ - wavy microchannel [35], ♦ - microchannel with cylindrical pin-fin array [57],

Fig. 5. Nusselt number enhancement with respect to friction factor augmentation of additively manufactured and conventional geometries; solid markers represent additively manufactured samples (figure reconstructed from above references)

X - Rib turbulators [6,49,50], □ - dimples [51–54], ◇ - angled groove [55], △ - pin fins [56], ▲ - rectangular minichannels [15], ● - teardrop and diamond minichannels [17], ■ - wavy microchannel [35], ♦ - microchannel with cylindrical pin-fin array [57].

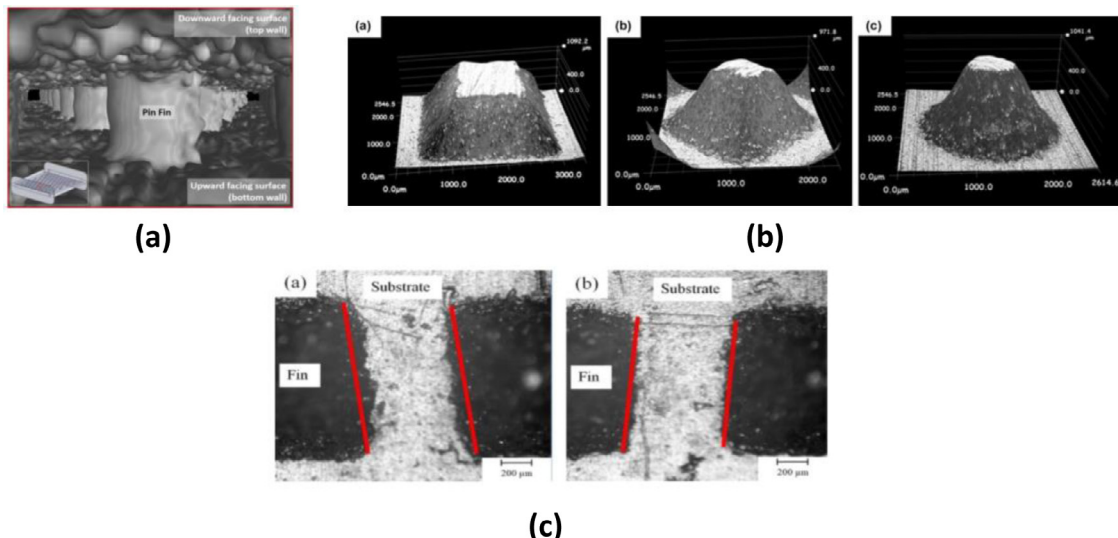


Fig. 6. (a) CT scan image of the pin-fin configuration in the microchannel with flow direction into the page [57], (b) pyramidal-shaped pin-fins with square, diamond and round base [63], (c) tilted flow passage geometry [61]. With permission to reuse from Elsevier.

but explores the qualitative constraints one has to consider while designing more complex pin-shapes in microchannels of height as low as ~ 1.5 mm in future.

Ferster et al. [59] investigated the thermal and hydraulic performance of four different pin shapes, namely, triangle, star and dimpled-sphere, printed in Inconel 718 via DMLS. The roughness on the pins and endwalls of these samples was apparent as observed in [57], but the intended shapes of the pin-fins were nearly captured while printing. The overall performance yielded by the triangular pin-fins was better than the star and dimpled-sphere pin-fin. The relatively smaller triangular pin-fins also provided similar thermal-hydraulic characteristics as cylindrical pin-fin arrays investigated in [57] for same wetted surface area, indicating that the application of triangular pin-fins could save material. This study exhibited the potential of fabricating different micro-pin fin shapes but also suggested that complex designs might not yield in the best performance.

Cormier et al. [60], Dupuis et al. [61], Farjam et al. [62] and Dupuis et al. [63] characterized the thermal and hydraulic performance of pyramidal pin fins with square, circular and diamond bases printed in aluminum via Cold Gas Dynamic Spraying (CGDS), as shown in Fig. 6b. Different pin-fin heights, fin-spacings and fin-arrangements (inline and staggered) were explored and the flow structures were also identified using μ PIV technique. Double recirculation flow patterns typical of uniform cross-section cylindrical pin fins and banks of tubes were observed which were however modified due to imperfections (tilt) caused in the fins during manufacturing (Fig. 6c). For the experiments conducted even at a low Reynolds number range of $Re_{dh} \sim 500$ to 2000, significant averaged local turbulence intensities of up to $\sim 15\%$ to 30% were observed over different locations. While the pressure drop was primarily governed by the turbulent kinetic energy in the fin wake, heat transfer coefficient was considered to be influenced by both the turbulent kinetic energy as well as turbulent intensity (strength of velocity fluctuations relative to average velocity at a location).

Additively manufactured twisted and chevron mixers printed in cyanate ester resin via Continuous Liquid Interface Production (CLIP) were investigated by Kwon et al. [64] in a tube with 180° bend. When compared against smooth channel (without mixer), the additively manufactured mixers yielded half of the thermal resistance of smooth channel at low Reynolds number ($Re_{dh} < 1000$) but almost similar value at higher Reynolds numbers. Rastan et al. [45] fabricated minichannels containing the rectangular winglets (vortex generators) and investigated the thermal-hydraulic performance of the samples with water as the working fluid (Fig. 7). At the highest Reynolds number ~ 1380 , heat transfer enhancement of about three times with respect to smooth channel (without winglets) was provided at the cost of 8.7 times higher pressure drop. Prior to experimental testing, different minichannels were prepared using DMLS (AlSi10Mg) and Electron Beam Melting (EBM, in Inconel 718). EBM produced clogged channels when dimensions were below ~ 1.5 mm and rendered poor surface finish to the samples. Since DMLS yielded better part quality at desired dimensions, it was finally used to prepare the test samples. Fig. 8a shows the capability of AM in printing different types of heat transfer augmentation features on a substrate. Searle et al. [65] and Unger et al. [66] also demonstrated the use of AM technologies to manufacture internal pin-fin (Fig. 8b) and novel external-fin designs, respectively.

While most of the studies mentioned above demonstrated the ability to manufacture micro-scale features, it is interesting to note that there are several studies which reported the fabrication of fully-functional integrated HX and compared to its traditionally made counterpart. Lynch and co-authors [67–69] manufactured liquid-to-air louvered plate-fin heat exchanger in AlSi10Mg via SLM and compared it with commercially used similar HX made by

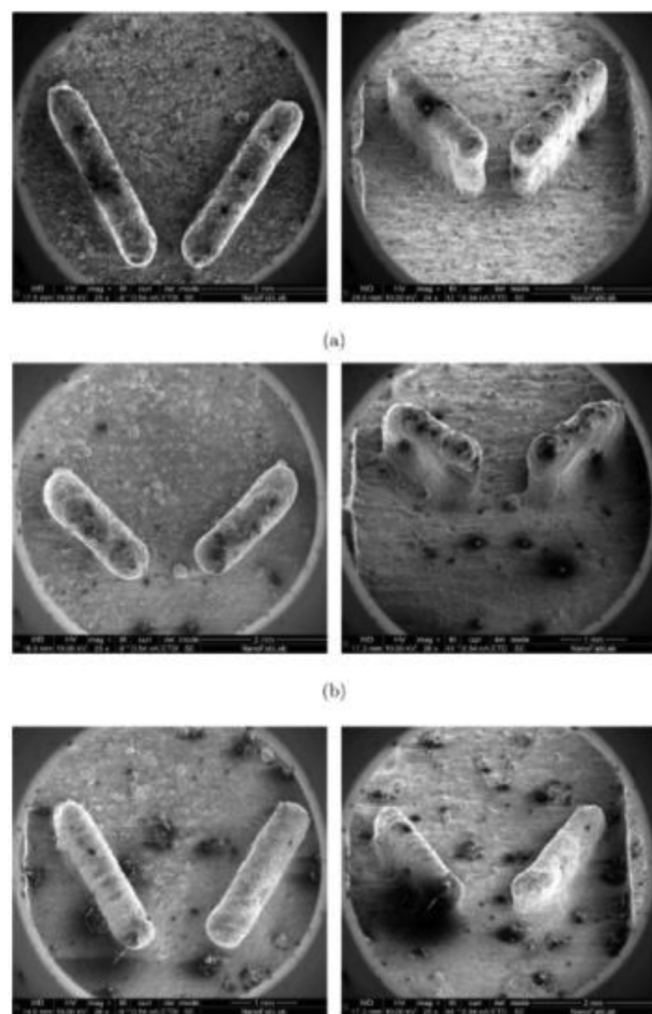


Fig. 7. SEM image of winglets for varying length, height and angle [45]. With permission to reuse from Elsevier.

brazing and stamping. The additively manufactured part (Fig. 9a) was similar to traditional counterpart except for some geometrical modifications which were necessary for successful printing. To further augment the performance, another HX with small winglets (vortex generators) attached on the air-side was also fabricated. The roughness in the additively manufactured parts was about an order of magnitude higher than traditional HX, a trend which was observed for several other printed parts mentioned above. The monolithic build of the additively manufactured HX was successful but cracks on about 20% of inlet and outlet face were observed (Fig. 9b). The heat transfer enhancement provided by additively manufactured samples was 10% - 14% higher relative to traditional HX but incurred about twice the air-side pressure drop.

2.4. Cellular materials

Cellular materials contain voids which enhance the structural and functional properties of the material with respect to its monolithic solid-phase material block. Commercially procured open-cell metal-foams are one such cellular materials which have been reported to possess good thermal and mechanical load-bearing capabilities. These metal foams are a dense network of metal-fibers which promote flow mixing, thermal dispersion and exhibit high permeability, surface area-to-volume ratio, effective thermal conductivity and interfacial heat transfer coefficient [70]. The metal

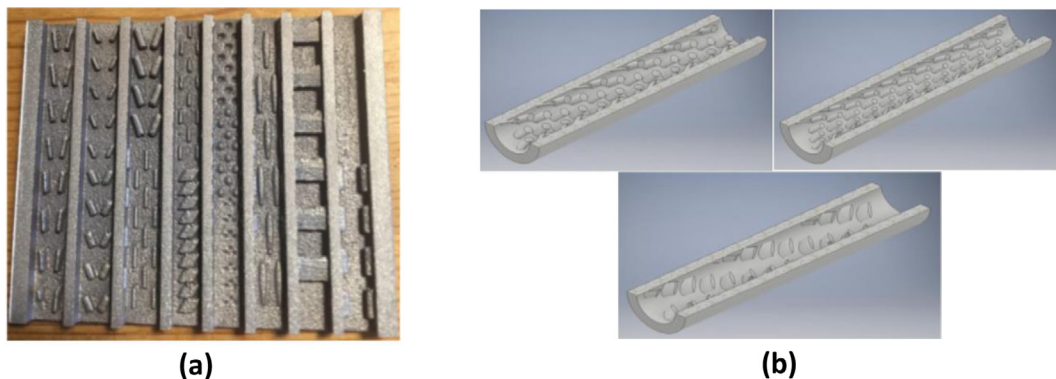


Fig. 8. (a) Different types of passive heat transfer techniques printed via DMLS [45], (b) pin-fin designs [65]. With permission to reuse from Elsevier.

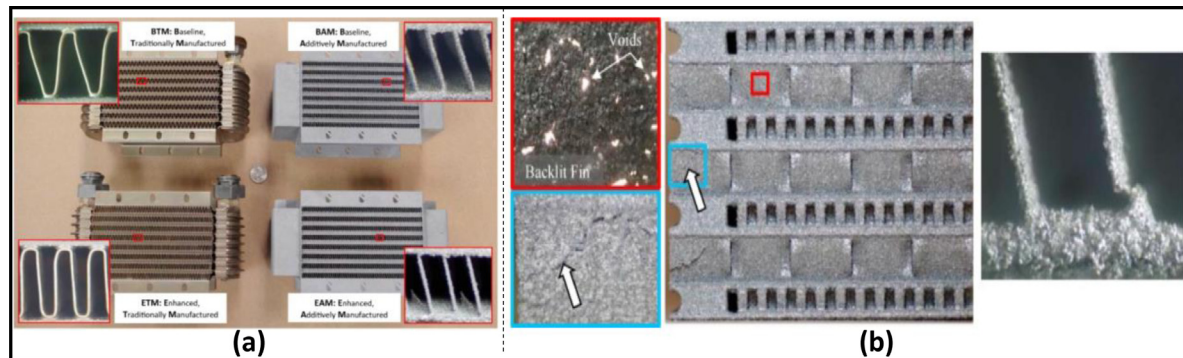


Fig. 9. (a) Traditional HXs alongside additively manufactured HXs, (b) cracking at the air-side fins and voids in fin thickness [67]. With permission to reuse from Elsevier.

foams are employed in heat exchangers, energy absorbers, air/oil separator, filters, acoustic damping, electrodes, chemical reactors, etc. The detailed information of thermal and hydraulic characteristics of these metal foams already exist in the literature. Despite the many advantages that metal-foam offer in thermal management applications, the major drawbacks include the irregular and random cell arrangement due to traditional manufacturing processes and difficulty in bonding these on the heated substrate which is to be cooled.

Cellular materials of periodically arranged unit cells have been extensively explored by the structural engineers because the customized unit-cell topologies can provide better strength and stiffness properties than stochastic open-cell metal foams [71]. It is only recently that the heat transfer and hydraulic properties of different user-defined unit-cell topologies are also being explored. Additive manufacturing not only provides freedom in preparing lattices with customized morphological parameters but also print the entire cellular structure on the substrate, thereby, eliminating the additional thermal interface material resistance.

Chaudhari et al. [72] and Ekade et al. [73] investigated the Octet unit cell topology and reported the effective thermal conductivity, permeability, inertial coefficient, friction factor and heat transfer coefficient for porosities ranging between 0.62 to 0.95. At a fixed porosity, the permeability and inertial coefficients were significantly higher than stochastic metal foams, but the friction factor was either lower or comparable to metal foams. For the three test samples printed in AlSi10Mg via DMLS, the transition of Darcy to non-Darcy regime was reported to occur at Reynolds number, based on square root of permeability ($Re_K = u\sqrt{K}/v$), of ~ 7. Due to similar thermal performance, lower pressure drop and better mechanical properties, Octet unit cell topology was considered a good candidate to replace stochastic metal foams in multifunctional HXs.

The Octet unit cell was reported to enhance the pool boiling heat transfer coefficient significantly with respect to plain surface due to increased surface area and nucleation site density [74]. The roughness generated on the samples while printing via SLM was considered as possible active nucleation sites for boiling. It is worth noting that there are attempts to investigate the pool boiling phenomenon on surfaces manufactured by different AM technologies [75–77], where the fabrication of micro-features (fins and cavities) on these surfaces is being explored. Single droplet impact cooling on heated surfaces with embedded small-scale clavate and globe-shaped fins having height of about ~0.6 mm to 2.5 mm were investigated by Wang et al. [78].

Rhombi-octet (Fig. 10a) and Rhombic-dodecahedron unit cell topologies were investigated for their thermal and pressure drop properties by several authors [79–83]. A wide range of unit cell sizes were investigated but the typical porosity of all these samples was within ~ 0.84 to 0.86. Mixed success was achieved in enhancing the performance relative to baseline configurations in these studies depending on the heat-transfer mode. Rhombi-octet heat sink provided higher efficiency index ($\eta = Nu/f^{1/3}$) and about ~ 5.5 times higher effective thermal conductivity than aluminum foams when the comparison was made with metal foams having similar fiber dimensions. It also yielded in higher heat transfer than helical inserts when employed in cylindrical water-cooled plate with both, fully and partially filled configurations. Ho et al. [81] fabricated commercial-scale Rhombi-octet lattice HX which provided better air-side heat transfer coefficient than conventional fin-tube HX at higher pumping power conditions. Rhombic-dodecahedron yielded 60% higher heat transfer coefficient with the corresponding increment of 66% in pressure drop with respect to stochastic metal foams of similar porosity and pore density in forced convection experiments but underperformed relative to simple longitudinal pin-fin arrangement in natural convection set-up [82]. While

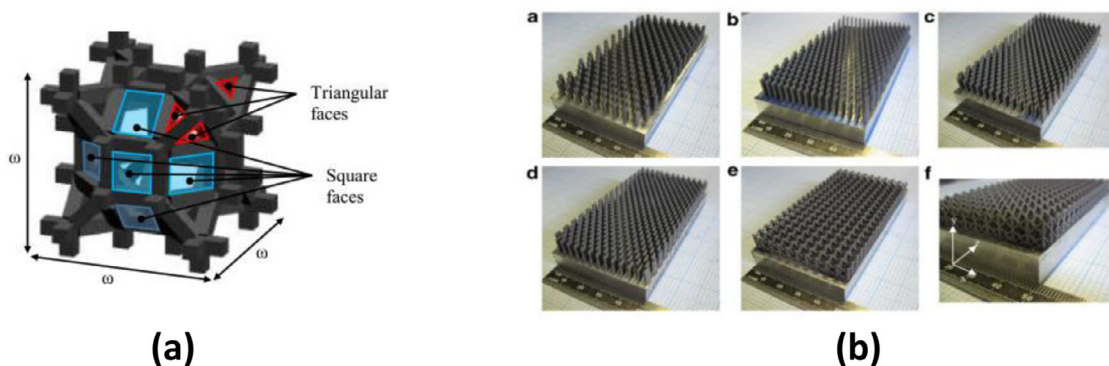


Fig. 10. (a) Rhombi-octet unit cell with samples printed with the unit cell topology [81], (b) samples printed with different pin-fin shapes [84]. With permission to reuse from Elsevier.

enhanced surface-area is helpful in dissipating more heat due to improved fluid-solid interaction, the impedance offered to the fluid motion by dense fiber structure can undermine these benefits in buoyancy-dominated flows. Lattices do not always offer enhanced performance in forced-convection scenarios as well. Wong et al. [84] investigated the convective heat transfer and pressure drop characteristics of cylindrical pin, triangular pin, elliptical pin and lattice heat sinks manufactured via SLM (Fig. 10b). Lattice heat sink provided the lowest heat transfer coefficient for the investigated mass flow rate which the authors attributed to poor fin efficiency and inhibition in fluid-fiber interaction due to geometric orientation of the fibers. Airfoil shaped fins in study by Ho et al. [85] reportedly outperformed the circular pin-fins in terms of global Nusselt number values.

Klumpp et al. [86], Liang et al. [87] and Yun et al. [88] investigated the simple Cubic and face-centered cubic (FCC and FCCZ) unit cell topologies. Both experimental and numerical work was conducted to characterize the thermal-hydraulic properties of these topologies. Since these unit cell topologies are fiber (often referred to as ligament or strut)-based, the effect of different fiber shapes (circular, rectangular and elliptical) and orientation angle with respect to the incoming flow was also investigated. Kagome and tetrahedral unit cell topologies can be conveniently manufactured by metal-wire and casting techniques. Recently, these unit cell topologies are being printed via additive manufacturing and tested for their thermal-hydraulic performance, especially in the sandwich-type configurations [89]. The possibility of using Kagome structures in the internal cooling channels of trailing edge of turbine blade is also being explored [90].

A relatively new class that is being investigated for convective thermal transport characteristics is that of bio-inspired cellular materials known as triply-periodic minimal surfaces (TPMS) [91]. These are mathematically defined surfaces that exhibit minimum possible surface area within specified boundaries and exhibit zero mean curvature. The geometrical and mechanical characteristics of TPMS has garnered significant attention for viability in tissue regeneration and orthopedic implants [92]. Some of the common TPMS topologies are Schwarz Primitive, Schwarz Diamond, Schoen Gyroid, Schoen I-WP, and Fischer-Koch S [93,94], shown in Fig. 11. These TPMS geometries can be produced as solid-network (also called skeletal TPMS [95]) and sheet-networks as described by Al-Ketan et al. [93]. TPMS divides a given volume into two congruent regions and closing of one of these volume gives solid-network whereas thickening of the TPMS gives sheet-network. TPMS based geometries have smooth profile and hence eliminates the stress concentrations which are generated at the junctions of strut-based topologies (Octet, Rhombi-octet, Rhombic-dodecahedron, Cubic, FCC, etc.). Moreover, sheet-TPMS exhibit very high surface area-to-volume ratio which is of particular interest to

the heat transfer engineers. Several studies have been dedicated to understanding the mechanical properties of sheet-TPMS and their performance relative to fiber/strut-based topologies [93,95–97]; sheet-TPMS offer superior mechanical properties relative to their strut-based counterparts. Graded TPMS having variable relative density, hence porosity, within the cellular material block are also being considered.

Permeability of different TPMS scaffolds is reported by several authors [98–105], but the flow velocities considered in these studies were mostly in the Darcy regime where the non-linear inertial effects were not considered. The employed flow rates are that of typical body fluids as these studies focused on the application of TPMS as orthopedic implant which requires the TPMS structure to be permeable enough for nutrient, oxygen, waste transport etc., and also strong enough to sustain mechanical load. Santos et al. [106] investigated high mass flow rates and reported the transition behavior of three TPMS, namely, Schwarz-diamond, Schwarz Primitive, and Gyroid, from Darcy to Forchheimer regime. The transition zone was narrow, and no particular transition Reynolds number could be identified. Forchheimer's law was deemed suitable for calculating the permeability because it gave values similar to those from the Darcy's law. Montazerian et al. [107] investigated cylindrical blocks of fiber-based lattices and TPMS to find that the TPMS were in general more permeable in longitudinal fluid flow direction. Both radial and longitudinal permeabilities were studied, amongst which radial permeability was suggested to be more appropriate for cell-ingrowth behavior prediction and geometry optimization.

Thermal conductivity of different TPMS topologies were studied by Abueidda et al. [108], Smith et al. [109] and Mirabolghasemi et al. [110]. Thermal conductivity of TPMS was found to be strongly dependent on the porosity of the considered topology sample which is in resonance with the results of stochastic metal foams. Schwarz-Primitive, Schwarz-diamond, Gyroid, and IWP were reported to have similar values of effective thermal conductivity at a given porosity or relative density [108,110]. Surface roughness, consideration of perpendicular or parallel direction with respect to the build direction (anisotropy) and adopted heat treatment methods post manufacturing which can alter the microstructure of material, were also found to have significant impact on the effective thermal conductivity of the product. Selo et al. [111] reported the thermal conductivity enhancement of about ~30–40% with respect to the as-built part by using different post treatments such as annealing, solution heat-treatment and T6-like treatment. Moreover, the graded cellular-structure also depicted spatially varying response to the different heat-treatment methods.

Very few studies exploring the potential benefits of the TPMS in forced convection configurations exist in the open literature. Al-Ketan et al. [112] numerically compared the thermal-hydraulic

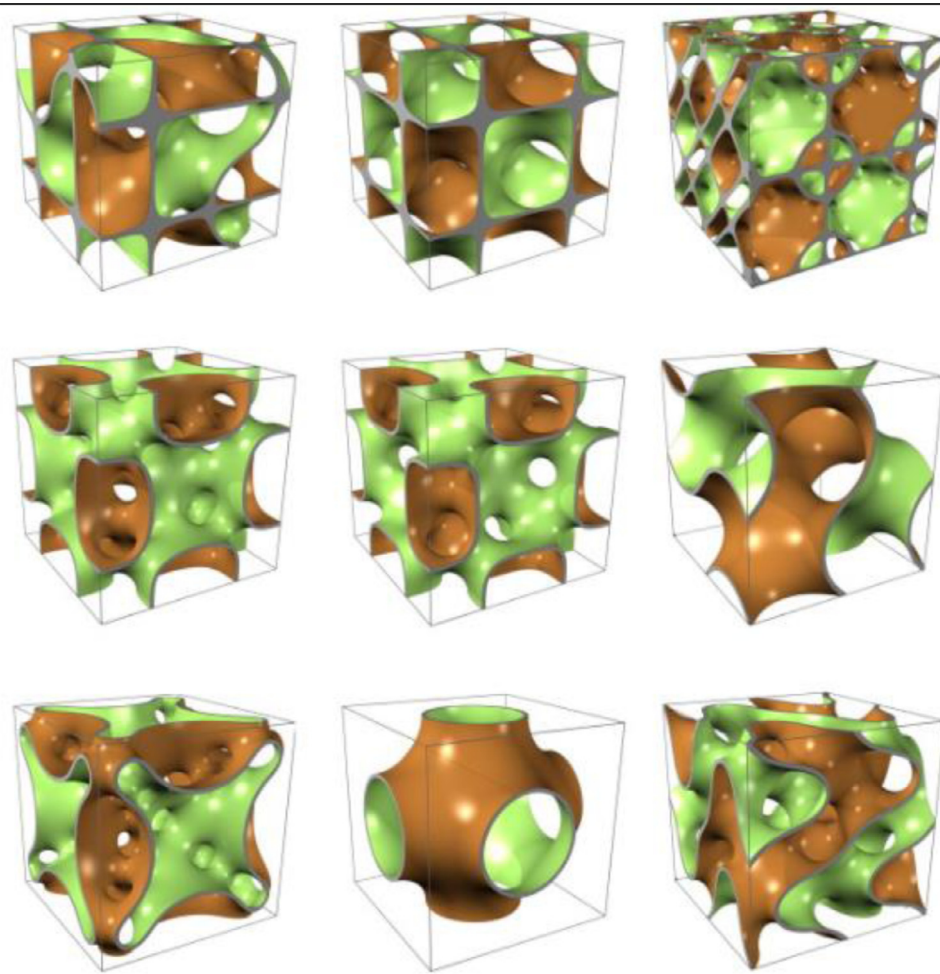


Fig. 11. Different TPMS topologies [94]. With permission to reuse from Elsevier.

performance of solid and sheet networks of Diamond and Gyroid topologies, the work which further explored the graded structures. Sheet Gyroid exhibited the highest overall heat transfer coefficient, U (hA_s , where h is the heat transfer coefficient and A_s is the wetted surface area) and highest pressure drop. The flow visualization depicted strong variation of the flow path and dispersion due to fluid-sheet interaction relative to solid-network geometries. In the graded expanding sample with porosity varying from 80–82.5% in the flow direction, about ~15.7% and ~27.6% reduction was observed in overall heat transfer coefficient and pressure drop, respectively. The reduction in the heat transfer was not as significant as in the pressure drop. Since there are several studies where the graded structures are examined for their mechanical properties, these thermal-hydraulic performance results are encouraging for obtaining optimum configurations where a graded structure can be conceived with acceptable heat transfer reductions but better hydraulic characteristics. This cannot only optimize the thermal-mechanical properties but also result in less material consumption and render less weight to the HX. It should be noted that the relative benefits of graded structure depend on the variable under consideration (mechanical, thermal, hydraulic, electrical) and the topology as it is possible that a particular graded topology might not be better than its corresponding uniform sample for a particular function/variable to be optimized.

Printed circuit HXs have emerged as promising candidates for applications in the Brayton cycles with supercritical carbon dioxide as the working fluid. The printed circuits are stacks of diffusion-

bonded plates that are chemically-etched with microchannels of different shapes such as straight, serpentine, zigzag, and trapezoidal [113,114]. These printed circuits have been proven to endure very high pressures and temperatures. They also have high surface area-to-volume ratio which results in enhanced convective transport. Since porous media has superior heat transfer and mechanical properties, these lattices can be explored as an alternative for printed circuit HXs. Recently, Li et al. [115] compared the flow and thermal transport properties of two TPMS topologies, Gyroid and Schwarz-D topologies with conventional printed circuit HX. The flow-field of the three structures was numerically analyzed in turbulent regime using k-omega SST turbulence model. The TPMS topologies provided 16–120% higher heat transfer coefficient than printed circuit HX at a given pumping power. The superior performance of TPMS topologies was due to enhanced turbulent kinetic energy and large surface area density. Additively manufactured HXs based on continuous TPMS topologies could be explored further as an alternative to the printed circuit HXs because of their potential to yield in better thermal characteristics. Although one should also investigate the cost of manufacturing for above processes and concepts.

Kim et al. [116] proposed a volumetric distance fields (VDFs) approach to design various types of compact HXs which could help in constructing application-oriented HX with desired features and also provide an estimation of the possible defects which might occur while printing. Defects such as high surface roughness was noteworthy in the microchannels, and turbulence-enhancing fea-

ture studies discussed in the Section 2.3 and 2.4 above. Similarly, cellular structures also suffer from this unintended roughness due to sticking of powder material. Other defects which are generally reported in cellular geometries are stair-case effect, cracking, micro-voids, pore-obstruction, tunneling-porosity etc. [112,117,118] which depend on the process parameters, geometrical dimensions, and material. Careful control over these parameters can result in better product finish, at least for the dimensional limits that are currently realizable. This can be beneficial in claiming the repeatability of the additively manufactured products and thus the results can become more consistent for similar geometries in the literature related to AM, a characteristic which cannot be assured about stochastic metal foam data with certainty.

There is no unanimous and definite opinion on the morphological parameter (pore size, pore definition, fiber size, fiber shape, representative unit cell shape), characteristic length for obtaining non-dimensional variables (common characteristic lengths are pore diameter, unit-cell diameter, square root of permeability), transitional Reynolds number from linear Darcy to non-linear Darcy-Forchheimer regime, transition from laminar to turbulent and its variation with pore-density and porosity, permeability values for different samples and their calculation methodology, etc. There is extensive analytical and theoretical framework which explains the flow and thermal transport in the stochastic metal foams, but the experimental data shows non-uniformity. The correlations and theoretical models which are derived by assuming some sort of geometrical representation for unit cell of metal foams also give different results. While the choice of characteristic length scales and calculation methodologies can vary according to the opinions of different authors (it can be based on physical explanations or may be on the scales that make the final data more consolidated and coherent, etc.), the issues of pore-definition, size and shape can be eliminated by incorporating periodic structures. Since the definitions that are currently being used to report the performance of cellular structures is borrowed from the porous media literature or metal foams (specifically for fiber-based topologies), proper characterization of regular periodic structures in these studies can make the data more lucid and reproducible.

Apart from the thermal-management applications mentioned above, TPMS are currently being investigated as spacers in the membrane distillation process for enhancing the heat and mass transfer [119–121]. The TPMS spacers provided a significant enhancement of more than 60% in the overall film heat transfer coefficient relative to the commercial spacers and mitigated the organic fouling due to its unique architecture. The possibility of using TPMS as static mixers in water treatment plants is also being explored [122].

Fig. 12 shows the normalized effective thermal conductivity as function of porosity for sheet-based and fiber/solid-network based cellular structures. Most of the sheet-TPMS have similar thermal conductivity values which are significantly higher than solid-Gyroid as well as conventionally manufactured stochastic metal foams.

2.5. Heat pipes

Heat pipes (HPs) are passive two-phase devices which exhibit high heat transfer rates with minimal temperature drop by utilizing the latent heat of vaporization of the working fluid. HPs are successfully employed as heat sinks and heat spreaders in micro-electronic devices, laser diodes, photovoltaic cells, aircrafts, space-radiators, etc. [123–127] due to their high effective thermal conductivity and heat dissipation capability. Fundamentally, HP consists of an evaporator section (attached to the heat source), adiabatic length (absent in some designs), and a condenser section (attached to the heat sink) in its architectural framework. The encapsulated leak-free HP container has the wick lining and the working fluid. Heat is conducted from the pipe-wall to the wick in the evaporator section where the liquid is transformed into vapor and carried away to the condenser section due to vapor pressure. The vapor releases the latent heat of vaporization in the condenser section and returns to the evaporator section via wick assisted by capillary forces. Gravitational, centrifugal, electrostatic and osmotic forces can also contribute as the driving forces [128].

Some common types of HPs investigated in the literature are vapor chamber, loop HPs, capillary-pumped HPs, annular HPs, rotating HPs, and gas-loaded HPs [128–130]. HPs are designed with various cross-sectional shapes (e.g. triangular, trapezoidal, curved rectangular, curved-triangular) where the corners develop the capillary forces, and in different materials (copper, stainless steel, polymer, silicon) [129,130]. Several types of working fluid such as water, methanol, n-pentane, isopropyl alcohol, acetone, ammonia, FC-72, etc. have already been investigated whereas combination of several fluids as a potential working fluid for HPs has also been proposed [131].

Capillary force is the main driving force for the proper functioning of an HP which is dependent on the wick structure. Screen mesh, sintered powder and axial-grooves are often employed as wicks in the HPs, which are basically porous media. Low porosity (smaller pore size) of the wick structure is desired to generate sufficient capillary pressure to push the fluid to the evaporator section and to achieve high thermal conductivity [134]. On the contrary, high permeability is required for proper fluid movement which is compromised at low porosities. Therefore, a trade-off between the permeability and capillary force has to be considered while optimizing the wick structure. High permeability along with large capillary forces are the ideal wick properties which screen mesh, sintered powder and axial grooves are not capable of providing simultaneously when employed individually. Some success in achieving these properties is gained by employing composite wick structures.

Micro-machining, broaching, extrusion-ploughing, plasma-etching, chemical etching and silicon-wafer bonding are reported manufacturing techniques for different types of HPs/wicks [129,135–137]. Axial grooved HPs have high thermal conductivity and permeability but weak capillary pumping pressure. The machining of grooves in long HPs is difficult and expensive. Sintered wick depicts excellent capillary pumping and thermal conductivity but low permeability. Sintered HPs are difficult to fabricate, and the resulting wick structure is random and heterogeneous. Fabrication of customized homogeneous wicks with enhanced thermo-fluidic properties and improved thermal contacts by manufacturing HP as a single component (elimination of thermal-resistances such as that between the HP and the condenser-side heat sinks, and between the pipe wall and porous wick) can be achieved by additive manufacturing technology, thereby, eliminating some disadvantages of the traditionally made HPs. Apart from the wick structures and overall design of the HP, its performance is dependent on several other factors such as working fluid, filling ratio, operating conditions, wettability of the wick, and position of evaporator/condenser-side relative to the body forces (gravity).

Very few studies have reported the performance characteristics of HPs manufactured via AM technologies. Ameli et al. [138] demonstrated that aluminum porous wick structure composed of regular Octahedral unit-cell topology having unit cell size of ~300 μm to 700 μm (Fig. 13a) could be manufactured via SLM with container and end-caps as a monolithic component. When compared to random porous wick structure composed of same unit cell topology, no significant differences were observed in the permeability values. The investigation was focused on characterizing the process and material of the HPs, and therefore, no through information on the thermal-hydraulic performance (except for per-

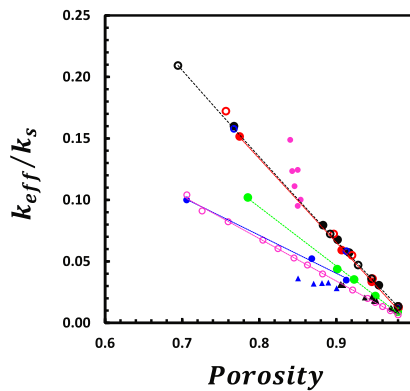


Fig. 12. Normalized thermal conductivity of different unit cell topologies as a function of porosity.
 ● - Octet [73], ● - Rhombi-Octet [79,81], ● - sheet-Gyroid [108], ● - sheet-Primitive[108], ● - sheet-CLP[108],
 ○ - sheet IWP[108], ○ - sheet- Neovius [108], ○-solid-Gyroid [108], ○ - sheet-S [108], ▲ - stochastic metal foam (Al)
 [132], ▲ - stochastic metal foam (FeCrAl) [133]

Fig. 12. Normalized thermal conductivity of different unit cell topologies as a function of porosity.
 ● - Octet [73], ● - Rhombi-Octet [79,81], ● - sheet-Gyroid [108], ● - sheet-Primitive[108], ● - sheet-CLP[108],
 ○ - sheet IWP[108], ○ - sheet- Neovius [108], ○-solid-Gyroid [108], ○ - sheet-S [108], ▲ - stochastic metal foam (Al)
 [132], ▲ - stochastic metal foam (FeCrAl) [133]

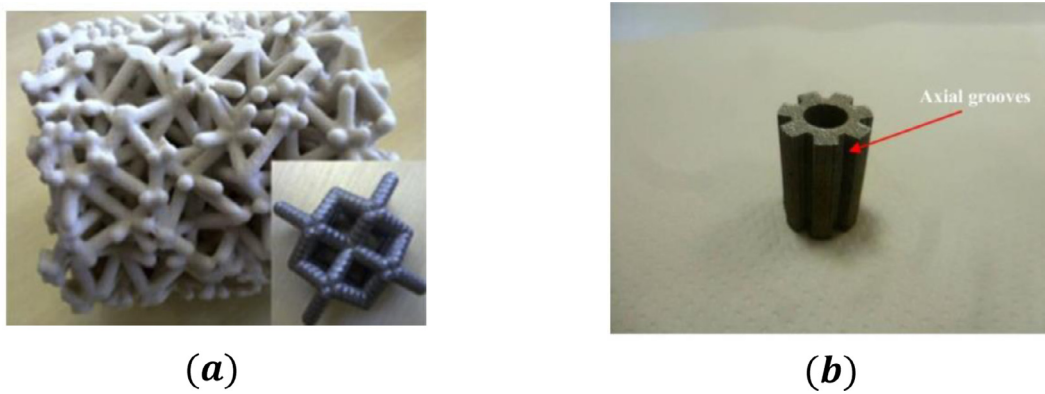


Fig. 13. (a) Octahedral unit cell wick shown in inset [138], (b) grooved-wick [139]. With permission to reuse from Elsevier.

meability values) was reported. This study was significant in bringing forth the potential of SLM to manufacture HPs.

Primary wick (porosity of ~0.17) consisting of grooves (Fig. 13b) was manufactured by Esarte et al. [139] and characterized for its wettability, capillary pumping and thermal conductivity. The stainless steel wick prepared via SLM for Loop Heat Pipe (LHP) to cool LED lamp yielded ~0.15 K/W resistance for a representative load of 80W. Ibrahim et al. [140] investigated oscillating HP consisting of four-interconnected layers of mini-channels manufactured in Ti6Al4V for various heat inputs, working fluids (water, acetone, Novec™ 7200, and n-pentane), and different orientations (vertical top- and bottom-heating, horizontal). Thermal resistance was dependent on the power-input, working-fluid and operating orientation. The destructive surface-quality testing showed roughness because of loose Ti6Al4V powder particles attached to sintered particles which the authors expected to decrease start-up power threshold and increase pumping power capability due to secondary wicking behavior. Similar secondary wicking of the partially melted particles and amorphous melt-regions was reported by Thompson et al. [141] in additively manufactured oscillating HP which yielded effective thermal conductivity of ~110 W/m.K at 50W.

Jafari et al. [134,142,143] thoroughly characterized the thermal and hydraulic properties of additively manufactured wick composed of Octahedral unit cell (porosity ~0.46) made in stainless steel via SLM. Effective thermal conductivity of the porous structure was found to be ~3 W/m.K and ~6 W/m.K when saturated with ethylene glycol and water, respectively. The transition of the

Darcy to Forchheimer regime was observed at permeability based Reynolds number $Re_k \sim 0.95$. When compared to traditional sintered, grooved, and weaved wicks from the literature, the 3D printed wick showed better capillary performance (expressed as the ratio of permeability and effective pore radius, K/r_{eff}). About 1-6 times higher K/r_{eff} ratio was reported for additively manufactured wick as compared to traditional ones. Effect of filling ratio of different fluids on the thermal performance with 3D printed wick in a flat HP, and rate-of-rise of different fluids was also investigated by the authors. Similar to the observations reported by Ibrahim et al. [140] in additively manufactured wicks and several other HXs reported in the previous sections, Jafari et al. [142] observed surface roughness which promoted surface area for thin film evaporation/condensation.

2.6. Turbomachinery

AM enabled cooling technologies have recently gained attention of researchers in the area of turbomachinery. High inlet temperatures to gas turbine of high-pressure stages are desirable for the overall efficiency. The maximum inlet temperatures, and thus the efficiency, are dictated by the survival thermo-mechanical load limits of the turbine components. Extensive research has been conducted to characterize the material, aerodynamic shape, internal/external cooling mechanisms, and mechanical properties of turbine blades to maximize the output. The motivation to find better material, designs and cooling mechanisms that might be

prohibitive to manufacture via convectional casting process has now diverted the focus of researchers to AM. This section reviews the studies that investigated thermal-hydraulic properties of turbomachinery-related components/concepts manufactured via AM.

Jet impingement, film cooling, transpiration cooling, internal channels featuring engineered roughness such as pin-fins or rib turbulators are some of the common techniques to cool different sections of turbine blades subjected to high heat flux while operating in hot-gas flow path. Thermal-barrier coatings (TBC) on the external surface are also employed as a protective layer from hot gases. The review of additively manufactured turbomachinery-related literature suggests that majority of the work has been dedicated to exploring the cooling mechanisms and designs while providing thorough characterization of designs, process parameters, and surface-roughness effects on the performance.

In film cooling, coolant from the compressor is pumped through the internal ducts of blade and bled from the film holes such that it forms an insulating layer between hot gases and blade-surface. The overall cooling is the result of film-cooling, internal convection (coolant flowing in internal duct carries away heat from blade-surface in its vicinity), and in-hole convection. Different hole-shapes have been analyzed in the past including a thorough investigation of its various attributes such as shape, inclination, length, expansion angle, and inter-hole spacings [144]. These holes are generally manufactured by laser-drilling, electrode or electrical discharge machining (EDM), and water-jet drilling [145], where the shapes or design forms that could be generated are strictly guided by the manufacturing limits of the process adopted.

The in-hole roughness can significantly influence the cooling effectiveness of the holes, which was shown by Schroeder and Thole [146] by measuring the adiabatic effectiveness ($\eta = (T_\infty - T_{aw})/(T_\infty - T_c)$, where T_∞ , T_{aw} , and T_c are mainstream, adiabatic and coolant temperatures, respectively), of similar shaped holes but different roughness manufactured via conventional CNC milling. In-hole roughness had negative effects on the effectiveness as the surface with highest roughness size exhibited about ~60% reduction in effectiveness relative to smooth hole at the highest blowing ratio ($M = (\rho_c U_c)/(\rho_\infty U_\infty)$, where ρ and U are density and velocities, respectively, and subscripts c and ∞ refer to coolant and mainstream, respectively) of ~3. In-hole roughness resulted in thicker boundary layers along the hole-walls, higher core-jet velocities and jet penetration angles of the discharged fluid which turbulently mixed with the mainstream flow thereby severely losing its cooling potential at the high blowing ratio. This study indicates that blowing ratio as well in-hole roughness which would manifest as by-product of AM are both parameters of investigation.

Similar type of holes built with different dimensions (scales) and orientations relative to build direction demonstrate different surface roughness and therefore are susceptible to provide different thermal-hydraulic characteristics. It is important to analyze the performance of micro-holes manufactured via AM at scales comparable to operational turbine blades as the roughness results of scaled-up models in laboratories might not be relevant in practical applications. Also, the holes on the blade surface are aligned in different directions, suggesting that the influence of build direction relative to sample when manufacturing these via AM cannot be neglected.

Several prior studies have reported the influence of build direction on the mechanical properties [147] and surface quality of the additively manufactured parts. Build direction dictates the stair-stepping effect and anisotropy in mechanical properties [148]. Also, a different support generation scheme needs to be adopted for different build direction to ensure successful build and minimum deviations from intended designs. Cylindrical-shaped channels were

additively manufactured by Snyder et al. [17] with three different build directions, which were: (a) channel axes parallel to the build plate (horizontal), (b) channel axes 45° to the build plate (diagonal), and (c) channel axes perpendicular to the build plate (vertical). The circular channels printed with the vertical direction yielded in the best tolerance value and the least surface roughness of $R_a \sim 8.40 \mu m$, whereas the internal roughness by horizontal and diagonal build direction was about $\sim 16 \mu m$. The downward-facing surface layers of the channels that are printed directly on the unsintered powder material demonstrate higher roughness than the upward-facing surfaces [149]. Choosing an orientation where the internal surfaces are facing upwards can yield smoother surface profiles and improved surface quality [150].

An attempt to analyze the effect of both dimensional scales and orientation was made by Stimpson et al. [151], where the authors printed different test coupons with engraved row of laidback fan-shaped hole in nickel based alloy. The different test-coupons had holes with dimensions akin to that found in real turbine blade (1x), scaled-up version of the real holes by a factor of two (2x) and these two dimensional scales built with hole axis aligned vertically as well as at angled (21° to horizontal) direction. Both smaller and larger sized holes showed blockage in coupons built at an angle, with the problem being more profound in smaller holes. The roughness and blockage varied within different samples (Fig. 14) and also amongst different holes of the same sample. In-hole roughness was supportive in enhancing the in-hole convection but reduced the film effectiveness due to increased jet momentum and turbulence exiting the hole which resulted in jet lift-off, hindering the formation of coolant blanket on the surface. Comparison to smooth holes built via EDM showed that the additively manufactured coupons were less effective in cooling a surface proving the functional superiority of conventionally made parts. According to the authors [151], the inconsistencies in the printed dimensions with respect to the intended design and realization of desired cooling performance requires strategic implementation of dimensional scaling, alternative cross-section specification, and inclusion of build direction effects. Similar coupon configurational scheme involving 1x and 2x samples built with vertical and angled orientation was adopted by Stimpson et al. [152] to investigate the cooling performance for both cross-flow and counter-flow set-ups. 2x vertical coupon had the lower effectiveness in crossflow configuration whereas other coupons were not very sensitive to the relative flow direction.

Five novel designs including baseline-shape, console, crescent, oscillator, spiral and tripod film cooling hole geometries printed in nickel alloy with dimensional deviation of metering area of holes up to ~20% for the largest geometry were investigated by Snyder and Thole [153] at engine-relevant conditions. The coolant coverage, which was impacted by the geometric deviations at hole exits, was more uniform for console, crescent and tripod holes because of closed packing of the hole outlets. In-hole convection was reported to be the major deterministic factor for the overall performance of the hole geometries.

AM is a complex process involving many variables which can determine the final surface characteristics of the printed part. The above studies have focused on determining the in-hole roughness effect on film effectiveness by keeping process parameters same but varying build orientations and scaling of the base geometry, very few studies have reported the effect of different process parameters on the film cooling hole performance. Snyder et al. [154] showed that variations in laser power, laser speed, and hatch distance could change the internal surface roughness by ~50% while significantly impacting the friction factor but minimally influencing the heat transfer enhancement. Optimizing parameters to create rough surface can reduce the coolant consumption by ~75% with respect to smooth surface under constant pressure ratio

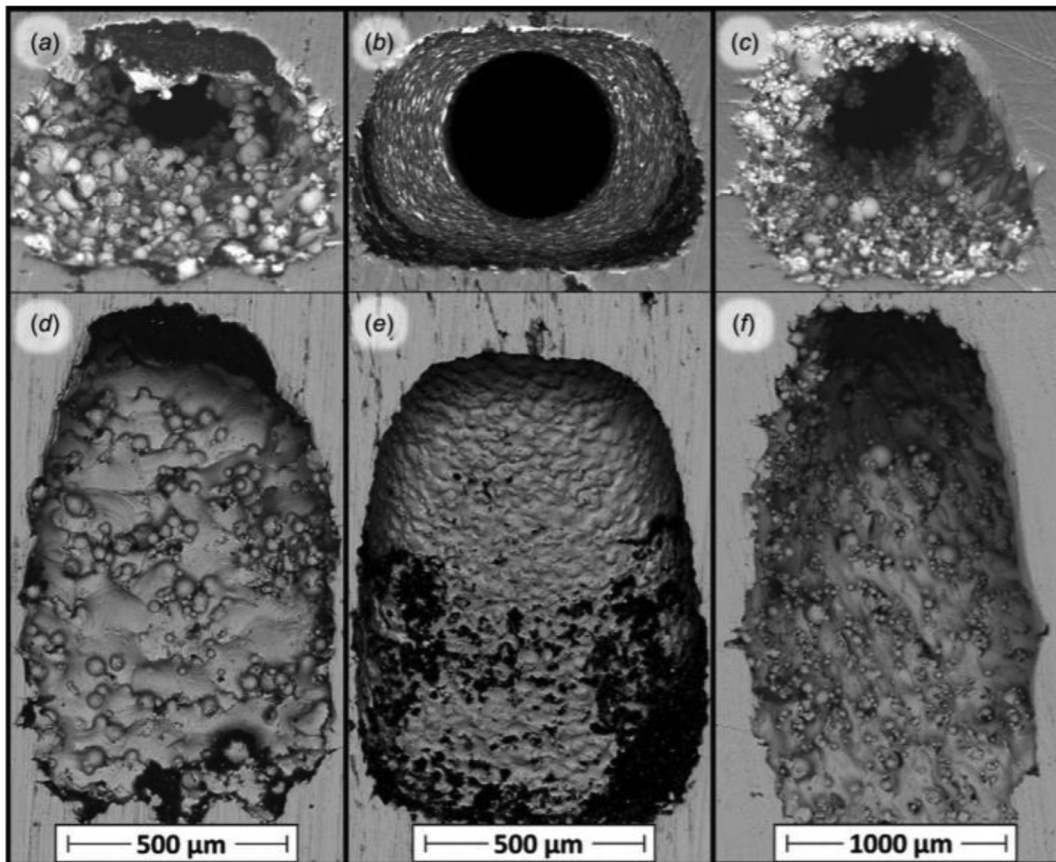


Fig. 14. SEM micrographs of film cooling holes showing roughness for 1x and 2x samples manufactured in vertical and angled orientation [151]. With permission to reuse from ASME.

condition. Significant cooling effectiveness reduction was observed for rough in-hole geometries.

The higher sensitivity of friction factor to the process variations than that of the heat transfer was reported by Kirsch et al. [155]. The repeatability of manufacturing process was checked by printing rectangular and wavy channels using different machines and material. Repeatability was poor for more complex wavy channel which showed non-uniform hydraulic diameter along the length of the channel. Shifting to a different material incurred about three times higher friction factor. Heat transfer and friction factor were found to be more influenced by effective channel hydraulic diameter than the roughness. The different surface roughness profiles generated by varying the laser power, laser speed and hatch distance in a study on similar geometry [156] showed the friction factor was the highest for the roughest channel but the Nusselt number was not higher with respect to relatively smoother cases. This was due to the roughness morphology where the shape of the roughness reduced the convective efficiency and also the reduction in fin thicknesses of the internal channels decreased the fin efficiency. The loosely attached powder to the surface may not be very effective in conducting the heat from the surface due to poor contact. Effect of process parameters such as hatching and contour effects were further detailed by Snyder et al. [157]. Numerical modelling of predicting the flow characteristics in additively manufactured rough surfaces is also being explored [158].

Internal cooling channels described in section 2.2 were built at angle of 45° to ensure the successful build while providing the necessary support to the part without requiring internal supports in the microchannels which could not be removed. The build direction has significant impact on the achievable dimensional ac-

curacy which also depend on the original CAD model sizes. Some microchannels have been reported to be built at 0°, and 90° as well but the angles lying between these values were not typically explored. To bridge the gap, Wildgoose et al. [159] also analyzed the build at 30° and 60° along with the aforementioned angles for varying circular channel diameters. For producing the circular channels at angles below 60°, some shape modifications were required to ensure the manufactured part is closer to the intended design. Similar pressure losses were incurred in the channels with same diameter built between 60° and 90°.

Transpiration cooling involves forcing of coolant through a porous wall to form a coolant layer between the outer wall and hot mainstream gas. Transpiration cooling provides higher cooling efficiency than film cooling with less coolant consumption due to large specific area available for heat dissipation and more uniform coolant coverage by discharge through high density of micro-scale holes as compared to discrete film cooling holes. Transpiration cooling became relatively unpopular for consideration in operational working turbine components because the porous media generated by conventional foaming, sintering, metal-wire weaving and laminated porous media approaches would not satisfy the criteria of acceptable porosity, design complexity, mechanical strength, and fabrication ease simultaneously. AM is now being considered by several investigators for generating uniform and high strength porous media with predictable performance for transpiration cooling. For example, Min et al. [160] investigated additively manufactured samples with array of round holes (perforated plates), sphere-packing (analogous to sintered particle block), wire-mesh, and blood vessel shaped configurations with an aim to increase the area for coolant discharge with lower porosity and high mechani-

cal strength. Three different injection ratio ($M = (\rho_c V_c)/(\rho_\infty U_\infty)$), where V_c is the average cross-sectional velocity of coolant flow in transpiration area) values of ~ 1.2%, 2.4% and 3.6% were investigated. Amongst porosity, internal solid-fluid interface area, and outlet area at the surface, the cooling performance was most significantly impacted by the internal wetted surface area. The comparison of local cooling characteristics of transpiration technologies with the film cooling holes reveled that the peak effective for film cooling occurred near the coolant outlet whereas for transpiration cooling it was in the central area of the porous structure.

Perforated plates having cylindrical holes is simple yet effective transpiration cooling design investigated by several authors with different hole sizes, pitch values, inline/staggered hole arrangement and hybrid type set-up with partition walls [161,162]. The perforated plates were capable of providing the uniform coolant protection even when separated by partition walls. Smaller pore sizes resulted in higher cooling effectiveness but lost mechanical strength due to stress concentration at hole edges. Trade-off between both these parameters have to be considered while choosing optimal configuration. Huang et al. [162] showed the additively manufactured porous plate with partition walls possessed about ~440% higher ultimate tensile strength than sintered porous material but lower cooling efficiency at higher injection ratio (~3%) due to film layer detachment.

An issue that can undermine the efficiency of transpiration holes is the blockage due to dust deposition which is very difficult to quantify in non-uniform sintered porous media. Yang et al. [163] utilized numerical scheme to predict the performance of perforated plate with different probability of blockage of holes and showed that upstream zones were more sensitive to the blockage as compared to downstream ones. The CAD model assisted additively manufactured geometries open more possibilities to predict the blockage behavior using numerical schemes.

Limited literature pertaining to the transpiration cooling employment via AM means has been presented so far by the investigators, but the results are encouraging to pave ways for future research in this field. Other cooling configurations such as parallel channels with inline wall jets, effusion holes with jet impingement for double-wall combustor liners, and incorporation of novel wavy trailing edge in the turbine blades manufactured via AM has been put forward by several authors with proof of better results than the baseline configurations [164,165]. While the design space has been rendered very flexible by the AM, authors like Chia et al. [166] developed oxide dispersion strengthening (ODS) coating for the high temperature turbine coatings using Direct Energy Deposition (DED) AM technology. The additively manufactured coating exhibited formation of stable oxide scales which also had excellent mechanical properties. The study proves that material/coating development is a field in which the AM technologies can progress into.

2.7. Jet impingement

Jet impingement technology is known for its high heat dissipation capabilities. Single impinging jet of fluid on a heated surface can yield very high stagnation heat transfer coefficient which decays away from the impinging spot on target plate. The uniformity of temperature distribution in such case can be ensured by using an array of jets. Also, the local hot spots can be managed by adjusting the relative position of nozzle to the target plate. Since the jet impingement technology involves direct communication between the working fluid and target surface, the problems associated with thermal contact resistances observed in other cooling technologies is not present. Jet impingement technology is capable of dissipating heat flux density of about 1820 W/cm^2 at pressure losses of around ~241 kPa[25]. Heat sink thermal resistance employing jet

impingement technology is typically of the range $\rightarrow 0.033$ to $0.203 \text{ Kcm}^2/\text{W}$.

Section 2.2 discusses the high heat dissipating capability of microchannels due to high heat transfer coefficient and large surface area. Several authors have attempted to increase the overall performance of the microchannels by reinforcing it with the micro-jets, thereby bringing together the benefits of high stagnation heat transfer coefficient of microjets and large surface area of micro-channels. Han et al. [168] compared hybrid (microjet + microchannel) configuration manufactured via convectional Deep Reactive Ion Etching (DRIE) and thermal conductive bonding with microchannel (MC) and microjet (MJ) configurations and found that hybrid configuration was capable of providing about ~20% and 5% lower temperature than MC and MJ, respectively. Very high local and averaged values of heat transfer coefficient values were reported by the authors for hybrid configuration. AM technology allows one to realize complex designs of hybrid models which otherwise could be very difficult by conventional means.

Kempers et al. [169,170] investigated hybrid (MJ+MC) configuration having microjets of hexagonal cross-section feeding the impinging fluid (water) to the target surface manufactured via proprietary AM technology MICA Freeform. The confining walls of the jet act as fins as well guide paths to redirect flow upward into central microchannel after impingement. Hybrid configuration provided about ~6% higher thermal-hydraulic performance enhancement ($h/\Delta P$) than MC and MJ.

Hot spot targeting can be achieved by proper designing of the nozzle array. The chip-coolers generally consist of inlets for feeding coolant to different nozzles, outlet which collects the coolant after impingement, and array of jets/nozzles. The entire assembly plays a crucial role is determining the overall cooling efficiency of the system. Nozzle diameters, nozzle number and distance from the target surface are all variables for investigation. Analysis of novel jet-array and hybrid assemblies manufactured by additive manufacturing technology are reported by several authors such as Wei et al. and Gonzalez-Valle et al.[167,171–173]. The design concepts of the investigated configurations in [167] are shown in Fig. 15. Wei et al. [171] reported thermal resistance of about $\sim 0.16 \text{ Kcm}^2/\text{W}$ for pressure drop of about 30 kPa.

Three different nozzle configurations were manufactured by Kwon et al. [174] in polymer via Cold Liquid Interface Production (CLIP) technology with jet exit diameters of ~1mm. The configurations depicted heat flux dissipation of about $\sim 58.4 \text{ W/cm}^2$ and convective heat transfer coefficient values up to $17 \text{ kW/m}^2\cdot\text{K}$ when investigated for Reynolds number range $\rightarrow 1.87 \times 10^4$ to 8.77×10^4 . The avenues opened by the AM technologies to discover more packaging designs for electronic components and maximize the efficiency of cooling systems are many. The monolithic build of the systems also provide an added advantage of lowering the manufacturing cost and heat sink weight. The studies targeting the manufacturing of jet impingement assemblies by introducing novel design concepts are scarce, but the available literature suggests that the progress in this area is underway.

2.8. Numerical prediction of the flow and thermal characteristics of additively manufactured HXs

Prediction of the thermal-hydraulic performance of additively manufactured HXs (microchannels, lattices, film-cooling holes, etc.) is challenging because the printed geometries deviate from intended CAD models by virtue of the inherent surface roughness as well as inaccuracies in the critical dimensions defining a configuration. Since computations serve as an important tool for estimation of thermal-hydraulic performance of designed HX in comparison to existing configurations, the AM-induced defects in the printed sample should be taken into consideration while draw-

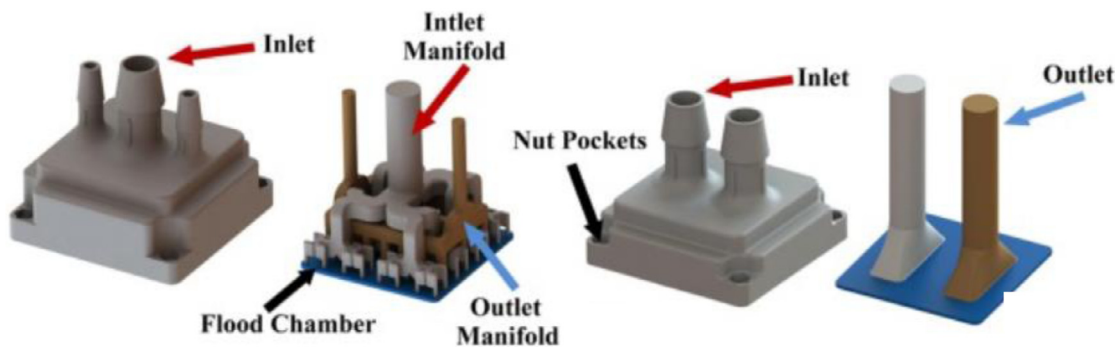


Fig. 15. Hybrid and traditional single outlet heat sink [167]. With permission to reuse from Elsevier.

ing conclusions on AM-parts' thermal hydraulic performance. Post manufacturing, the HX could be analyzed thoroughly via non-destructive techniques such as computer microtomography (CT scan), which has been successfully used by several authors to predict the thermal-hydraulic performance of stochastic metal foams reconstructed from CT scan data [175]. RANS-based simulations were performed by McClain et al. [158,176] on surfaces, the roughness characteristics of which were derived from a X-ray CT scan of coupons built via powder bed fusion technology. The simulated configurations involved the roughness profiles obtained from the upward- as well as downward-facing surfaces of the printed coupons. The authors also delineated the methodology to prepare the analog surfaces which replicated the flow modification properties of real printed surfaces by using deterministic shapes such as half ellipsoids or elliptical cones on the surfaces. In comparison to experiments, ellipsoid cone analog surface provided 15% and ellipsoids provided 50% deviation in friction factors. The modelling of surface roughness has been undertaken in the above studies and more analysis on analog surface generation can provide more insight into the local and average flow property variations.

Kirsch and Thole [33] performed steady-state Reynolds averaged Navier-Stokes equation using realizable k-epsilon turbulence model on baseline and optimized smooth wavy microchannels. The predicted friction-factor and Nusselt number was compared with that measured experimentally on samples printed via DMLS. The measured friction factor was about five times and Nusselt number was 1.5–2 times higher than that predicted by simulations. The discrepancies between numerical predictions and experimental findings were attributed to the surface roughness and steady-state nature of the applied governing equations.

Section 2.5 discusses the applicability of cellular materials in fabricating efficient and lightweight HXs. Both numerical and experimental investigations have been conducted to predict the heat transfer and pressure drop penalties in cellular material based HXs, however, the numerical studies are primarily conducted on the smooth (or idealized) CAD models. Several numerical studies provide the proof-of-concept for superiority of the proposed lattice as compared to previously investigated samples. Few studies such as that by Broughton and Joshi [83], compared the thermal-hydraulic performance of Rhombic-dodecahedron lattice predicted by conjugate laminar-flow based simulations with the in-house experiments on the same structure printed in metal via DMLS. Both numerical and experimental results were in good agreement with each other, however surface roughness aspect was not discussed. Liang et al. [87] also compared the numerically predicted heat transfer and pressure drop characteristics of FCC lattice with in-house experiments performed on lattice printed in resin via Stereolithography (SLA). Since the samples printed in resin yield smoother surface finish than that in metal, the numerically predicted endwall characteristics were in good agreement with the

experimental results. Contrary to the above study, the numerically predicted Nusselt number on Kagome-shaped lattice by Parbat et al. [89] underpredicted the experimental results on the same sample printed in Inconel 718. The numerical simulations were conducted in turbulent flow regime with k-omega SST turbulence model. The predicted Nusselt number was 10%–30% lower which was attributed to the surface roughness. However, there will be some contribution of the limitations of turbulence modeling in the prediction's deviation from their experiments. Above aspect of turbulence modeling is challenging to separate from the roughness effects.

The numerical studies focused on investigating the surface roughness effects on the flow and thermal exchange in additively manufactured lattices are still scarce. The incorporation of the actual surface roughness effects in simulated geometries is very challenging but extraction of data from real samples using CT scan methods can help in simulating the actual roughness or generate the corresponding analog surfaces with specific geometries to mimic the real turbulence field of the additively manufactured coupons.

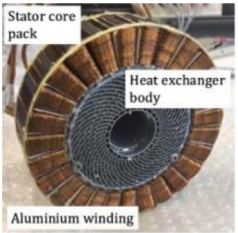
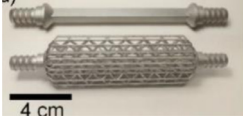
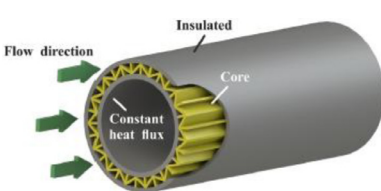
The roughness on the surface can be introduced artificially by mounting different turbulence promoting features. This architected roughness is uniformly employed on the surface and can influence the flow and heat exchange if their size is large enough to disrupt the boundary layer. Enhancement of heat transfer by employing the rib-turbulators in the cooling channels of gas turbine blades is one of the most common applications of deliberately adding artificial roughness to promote heat transfer between heated walls and the coolant. The introduction of tailored roughness modifies the local flow features by introducing secondary flows near the endwall as well as in direction normal to the bulk flow direction which essentially promotes flow mixing. Common flow features such as counter-rotating rotating vortices when the flow trips over these roughness features is reported in literature. The complex interaction of the secondary flows results in increased local turbulent kinetic energy which promotes heat transfer [177,178]. The introduction of these features in the flow path also leads to higher flow resistance which increases the pumping power requirements. Since the roughness induced by the additive manufacturing process has significant influence on the heat transfer and friction factor values, thorough investigation of localized influence of this roughness on the flow field and consequently on the heat transfer is required.

2.9. Concepts of some other HXs and future roadmap for the additive manufacturing

Table 2 provides a list of the studies that reported the manufacturing and experimental/numerical investigation of the additively manufactured HXs. This list, although not exhaustive, and the stud-

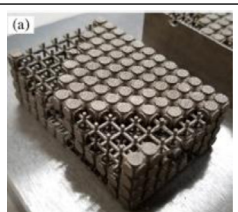
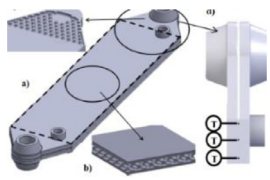
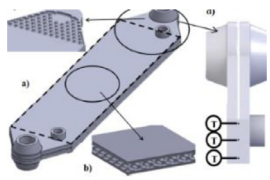
Table 2

Concepts of different HXs

Reference	HX design/manufactured sample	Concept/ additional comments
Arie et al. [187]		<ul style="list-style-type: none"> Air-to-water polymer HX having $\sim 150 \mu\text{m}$ thick walls accounting for only $\sim 3\%$ of the total resistance was manufactured Overall heat transfer coefficient $\sim 35\text{-}120 \text{ W/m}^2\text{K}$ was obtained for air-side flow rate of 3-24 L/s and water-side flow rate of 12.5 mL/s
Wrobel et al. [190]		<ul style="list-style-type: none"> Additively manufactured HX for thermal management of electric motors on high-altitude solar aircraft was investigated Higher fin density resulted in higher heat transfer as well as pressure drop. An optimum fin-density was proposed to be considered to strike a balance between the thermal management and pressure drop penalty
Lazarov et al. [191]		<ul style="list-style-type: none"> Topology optimized heat sinks were shown to have better performance than the lattice structures for thermal management of LEDs The optimized designs provided 17%, 21-23%, and 50% reduction in material, temperature, and operational cost, respectively
Luque et al. [192]		<ul style="list-style-type: none"> Four novel hierarchically-layered fractal-like volumetric solar absorbers were additively manufactured and investigated Overall thermal conversion efficiencies were comparable to conventional silicon carbide monolithic honeycombs
Moon et al. [193]		<ul style="list-style-type: none"> Additively manufactured structures were investigated as phase change material (PCM) thermal storage device The additively manufactured device yielded higher heat flux and power density than previous data
Sabau et al. [194]		<ul style="list-style-type: none"> Heat exchanger with non-circular cross section tubes with novel flow path, where the fluid path transitions between tube-flow to shell-flow, was manufactured The overall heat transfer coefficient of the novel HXs was $\sim 16\text{-}32\%$ higher than the baseline shell-and-tube HX
Sun et al. [195]		<ul style="list-style-type: none"> Heat transfer of additively manufactured sandwich-walled cylinders made with quadrangle and triangle cores was investigated The transition from laminar to turbulent regime occurred at Reynolds number of $\sim 2200\text{-}4100$ in the channels For a fixed heat transfer area, quadrangle core cylinder outperformed triangle core cylinder

(continued on next page)

Table 2 (continued)

Reference	HX design/manufactured sample	Concept/ additional comments
Takezawa et al. [196]	(a)  (b) 	<ul style="list-style-type: none"> The authors proposed technique to optimize the lattice density distribution via lattice structure approximation and gradient method The two multi-objective functions considered were reduction in pressure and temperature
Septet et al. [197]		<ul style="list-style-type: none"> Experimental investigation of flow boiling and condensation in additively manufactured HX was reported with n-pentane and water as the working fluid

*Figures reprinted with permission to reuse from Elsevier

ies reported in the previous sections highlight the widespread reach of the manufacturing capabilities of the AM technologies. The micro-electronic cooling equipment, industrial and commercial heat exchangers, aircraft thermal management systems, LED coolers, chemical-reaction intensifiers, turbomachinery cooling mechanisms, combustor liners, etc. are all being manufactured via AM with varying success. Many inherent challenges in manufacturing process are reported and the design solutions are being continuously proposed as well to overcome the same. Bernardin et al. [179] showed the potential of using CFD modeling tools and AM technologies in conjunction with each other by manufacturing twisted-tube HX via DMLS. Busse et al. [180] investigated additively manufactured cellular structures for heat transfer in catalytic reactors. The proper contact of cellular structures with the walls resulted in about ~ 3.5 times higher heat transfer efficiency relatively to loosely packed configuration. At lower gas flow rates, the open periodic cellular structures performed better than the randomly packed beds. Chekurov et al. [181] manufactured counter-flow HX with 144 flow channels in aluminum alloy which showed enhanced thermal transport due to inherent surface roughness with tap water as the working fluid. However, the authors reported a reduction in the performance level when the experiments were conducted after two months of the initial runs. Dede et al. [182] adopted topology optimization technique to manufacture heat sink for jet impingement air cooling. Topology optimized configuration could provide moderately high heat transfer for lower pumping power requirements as compared to some conventionally machined designs. Gerstler and Erno [183] proposed novel multi-furcating HX to meet the heat transfer and pressure drop specifications of commercial oil-cooler. For similar heat transfer and pressured drop characteristics, about ~ 66% and 50% reduction was observed in weight and volume, respectively, relative to commercial HX. Hymas et al. [184] additively manufactured polymer-metal composite HX where high conductivity fins passed through the low-conductivity channel walls. Although not related to thermal management field in particular, it is worth mentioning that biomedical sector is also extensively leveraging from the freedom to design freeform architectures using AM technologies [185,186].

Most of the studies reviewed above have employed SLM and DMLS to print the HXs in metal. Metals exhibit high thermal conductivity and excellent mechanical strength due to which they are more desirable for HXs. Polymers, too, have received considerable attention from research community as a viable alternative to manufacture HXs due to relatively lower weight, manufacturing cost,

antifouling and anti-corrosion properties [11]. The polymers, however, exhibit lower thermal conductivity, an issue which is being tackled by using polymer-metal matrix composites. The choice of the material majorly depends on the type and application of HX. For example, a stacked polymer cross-flow type configuration can be built where the walls can be made very thin to reduce the wall resistance, as shown by Arie et al. [187]. But the complete potential of cellular structure heat sinks or HXs are completely realized in conjugate thermal transport for which high thermal conductivity metals such as aluminum and copper are the most suitable. Ceramics are common materials used in high-temperature applications and several studies have reported the additive manufacturing of HXs using these materials [188,189].

The discussion presented in the previous sections clearly highlights the advantages of additive manufacturing in fabricating HXs. However, several disadvantages of additively manufactured HXs exist which need to be addressed. One of the disadvantages of the additively manufactured HXs is the dimensional inaccuracy and surface quality. Since the defects are a function of material and AM process itself, the AM product quality still largely remains unpredictable, and that detailed surface morphology characterization and CT scanning is required. For example, there is a general agreement in the thermal-hydraulic performance of the microchannels (including manifolds) and turbulence enhancement features such as pins-fins, rib-turbulators, etc. Such consistency of the results is yet not observed in the data of the corresponding additively manufactured HXs. Surface morphology of AM parts is one of the primary reasons for this discrepancy. The results of the additively manufactured HXs show a significant deviation from the standard correlations that were built for samples with their smooth counterparts.

Despite the inherent challenges, AM technologies have widened the design space and have demonstrated capability to manufacture complex and freeform designs with lesser weight and cost than conventional HXs. Few areas which still require thorough investigation, as far as HXs are concerned, are systematic and quantified effects of the process parameters on the surface quality (surface roughness in particular) in metal AM technologies, collaboration of numerical methods to optimize the HX geometry and evaluating its performance, progress in manufacturing of metals with high thermal conductivity such as copper which is more challenging to process relative to aluminum and nickel alloys, effect of surface roughness on the thermal and flow field in different types of HXs, potential of AM technologies in commercial-scale batch production of HXs with competing, if not higher, benefits over conventional tech-

nologies in terms of weight, cost, quality, thermal performance, etc. The existing literature suggests that the researchers are continuously trying to improve the existing technologies and bridge the gap between the intended and actual performance.

3. Conclusion

A thorough review of additively manufactured HXs is conducted and the thermal-hydraulic performance of the HXs has been analyzed relative to those made from the conventional manufacturing methods. Following conclusions have been drawn based on the investigation:

- 1 Surface roughness is the common and key-consideration in determining the thermal and hydraulic characteristics of the different types of metal HXs fabricated by powder bed-fusion technologies such as SLM and DMLS. Surface roughness incurred in additively manufactured HXs can be about an order of magnitude higher than that observed in same HXs built via conventional methods. Pressure drop is more severely augmented by inherent surface roughness in microchannels than the heat transfer. Therefore, a proper estimation of surface roughness and systematic collection of databases of corresponding process parameters is necessary. A significant deviation of manufactured dimensions which can be up to ~20% from the intended design can exist which also impact the thermal-hydraulic performance of the microchannel HXs. Some studies reported the pressure drop to be influenced by the resulting effective channel sizes rather than the roughness whereas several studies have reported the pressure drop as a strong function of surface roughness. Some authors have even argued that the relative roughness (ratio of roughness to channel hydraulic parameter) is more appropriate parameter to analyze the pressure drop characteristics. Critical analysis of the impact of surface roughness introduced by the AM technologies on the heat transport mechanism reveals that it's not only the size but also the shape and contact between powder particles and surface that determines the heat transfer efficiency of a HX.
- 2 The AM technologies have paved ways to manufacture optimized geometries which can be designed by coupled numerical tools and AM technologies. Very few studies have explored the possibilities of this collaboration, but the results are promising for future considerations. The programming controlled environment and additive mature of AM technologies has made the realization of complex optimized designs possible.
- 3 Material characterization is an important aspect which is very important but is mostly overlooked. Some studies have attributed the deviation in the analytical and experimental results to the incorrect/imprecise thermal properties of the additively manufactured material. A deviation of the properties such as final porosity and thermal conductivity of the actual sample from the vendor's database is possible and researchers should try to measure these in-house, if possible, to be certain. The characterization of the material property is as important as the surface properties.
- 4 Cellular structures depicted higher heat transfer and pressure drop than considered convective baseline configurations, but the overall relative benefit is dependent on the unit cell topology. Dominant heat transfer mechanism strongly determines the candidacy of a cellular structure in particular application. For example, a cellular network that performs the best in forced convective flows might not be the best in the natural convection set-up. Biomimetic technology can significantly nurture the possibilities of the AM technologies to make complex bio-inspired cellular structures. Sheet-based TPMS have higher surface area to volume ratio and high effective thermal conduc-

tivity which make them very attractive for conjugate thermal transport applications. Currently, the mechanical load bearing capability database is broader for these structures relative to their heat transfer and hydraulic characteristics, but the existing studies are evident of the ongoing progress in exploring these for advanced HXs.

- 5 Turbine technology community has also realized the benefits of AM and is exploring it for manufacturing film cooling and transpiration cooling mechanisms. The challenges of heterogeneous distribution and low mechanical strength of the porous media manufactured via conventional methods for transpiration cooling can reportedly be diminished by the capability of AM to fabricate high strength periodic cellular structures/porous media. Additively manufactured film cooling holes are more rigorously investigated as compared to transpiration cooling. The influence of surface roughness on the overall film effectiveness is complex and multi-dimensional. The in-hole surface roughness augments the in-hole convection due to improved turbulence, but the same mechanism proves detrimental for the film effectiveness because turbulence and increased core velocities leads to jet lift-off and ineffective film coverage. These effects are significantly augmented at higher blowing ratio which was typically ~3 in the reviewed studies.
- 6 Repeatability of additively manufactured HXs has also been questioned by some studies where the complex wavy channels showed geometric deviation when printed on different machines and with different material. Thus, a process parameter optimization of a machine with one material may not give same results for a different material.

The emergence of AM technologies as a viable option for manufacturing laboratory as well as commercial-scale HXs is evident from the existing literature. A significant enhancement in the thermal-hydraulic characteristics, and reduction in weight and cost can be achieved by AM. Although the AM technologies are superior to the conventional techniques in producing optimized and complex geometries, the part quality is relatively poor. This shortcoming of the AM technologies can definitely be used for benefit but only when concrete and systematic results are available. The current AM technologies cannot be considered a replacement for the conventional methods as such to entirely replace them commercially at the moment, but AM industry is functioning in parallel depicting its multi-dimensional benefits. A continuous progress in AM methods to mitigate the inherent limitations will make them a stronger alternative manufacturing technique for producing lightweight, multifunctional, and efficient HXs in future.

Declaration of Competing Interest

The authors of the submitted manuscript titled "State-of-the-art in heat exchanger additive manufacturing" wish to confirm that there are no known conflicts of interest associated with this publication and there has been no significant financial support for this work that could have influenced its outcome.

We confirm that the manuscript has been read and approved by all named authors and that there are no other persons who satisfied the criteria for authorship but are not listed. We further confirm that the order of authors listed in the manuscript has been approved by all of us.

We confirm that we have given due consideration to the protection of intellectual property associated with this work and that there are no impediments to publication, including the timing of publication, with respect to intellectual property. In so doing we confirm that we have followed the regulations of our institutions concerning intellectual property.

We understand that the Corresponding Author is the sole contact for the Editorial process (including Editorial Manager and direct communications with the office). He/she is responsible for communicating with the other authors about progress, submissions of revisions and final approval of proofs. We confirm that we have provided a current and correct email address which is accessible by the Corresponding Author and which has been configured to accept email from Elsevier.

References

- [1] J. Park, P.M. Ligrani, Numerical predictions of heat transfer and fluid flow characteristics for seven different dimpled surfaces in a channel, *Numer. Heat Transf. Part A Appl.* (2005), doi: [10.1080/10407780590886304](https://doi.org/10.1080/10407780590886304).
- [2] Y. Xie, H. Qu, D. Zhang, Numerical investigation of flow and heat transfer in rectangular channel with teardrop dimple/protrusion, *Int. J. Heat Mass Transf.* (2015), doi: [10.1016/j.ijheatmasstransfer.2015.01.055](https://doi.org/10.1016/j.ijheatmasstransfer.2015.01.055).
- [3] I. Kaur, P. Singh, S.V. Ekkad, Thermal-Hydraulic Performance Enhancement by the Combination of Rectangular Winglet Pair and V-Shaped Dimples, *J. Therm. Sci. Eng. Appl.* (2020), doi: [10.1115/1.4044169](https://doi.org/10.1115/1.4044169).
- [4] I. Kaur, P. Singh, S.V. Ekkad, Enhanced thermal hydraulic performance by V-shaped protrusion for gas turbine blade trailing edge cooling, *Int. J. Heat Mass Transf.* (2020), doi: [10.1016/j.ijheatmasstransfer.2019.119221](https://doi.org/10.1016/j.ijheatmasstransfer.2019.119221).
- [5] P. Singh, B.V. Ravi, S.V. Ekkad, Experimental and numerical study of heat transfer due to developing flow in a two-pass rib roughened square duct, *Int. J. Heat Mass Transf.* (2016), doi: [10.1016/j.ijheatmasstransfer.2016.07.015](https://doi.org/10.1016/j.ijheatmasstransfer.2016.07.015).
- [6] J.C. Han, Y.M. Zhang, C.P. Lee, Augmented heat transfer in square channels with parallel, crossed, and v-shaped angled ribs, *J. Heat Transfer.* (1991), doi: [10.1115/1.2910606](https://doi.org/10.1115/1.2910606).
- [7] S. Eiamsa-ard, K. Wongcharuee, P. Eiamsa-ard, C. Thianpong, Heat transfer enhancement in a tube using delta-winglet twisted tape inserts, *Appl. Therm. Eng.* (2010), doi: [10.1016/j.applthermaleng.2009.09.006](https://doi.org/10.1016/j.applthermaleng.2009.09.006).
- [8] M.R. Salimpour, Heat transfer coefficients of shell and coiled tube heat exchangers, *Exp. Therm. Fluid Sci.* (2009), doi: [10.1016/j.expthermflusci.2008.07.015](https://doi.org/10.1016/j.expthermflusci.2008.07.015).
- [9] A. Sinha, K. Ashoke Raman, H. Chattopadhyay, G. Biswas, Effects of different orientations of winglet arrays on the performance of plate-fin heat exchangers, *Int. J. Heat Mass Transf.* (2013), doi: [10.1016/j.ijheatmasstransfer.2012.10.034](https://doi.org/10.1016/j.ijheatmasstransfer.2012.10.034).
- [10] E. Klein, J. Ling, V. Aute, Y. Hwang, R. Radermacher, A Review of Recent Advances in Additively Manufactured Heat Exchangers, *Int. Refrig. Air Cond. Conf.* (2018) 1–10 <https://docs.lib.psu.edu/iracc%0Ahttps://docs.lib.psu.edu/iracc/1983>.
- [11] D.C. Deisenroth, R. Moradi, A.H. Shooshtari, F. Singer, A. Bar-Cohen, M. Ohadi, Review of Heat Exchangers Enabled by Polymer and Polymer Composite Additive Manufacturing, *Heat Transf. Eng.* 39 (2018) 1652–1668, doi: [10.1080/01457632.2017.1384280](https://doi.org/10.1080/01457632.2017.1384280).
- [12] B.M. Nafis, R. Whitt, A.C. Iradukunda, D. Huitink, Additive Manufacturing for Enhancing Thermal Dissipation in Heat Sink Implementation: A Review, *Heat Transf. Eng.* (2020) 7632, doi: [10.1080/01457632.2020.1766246](https://doi.org/10.1080/01457632.2020.1766246).
- [13] D. Jafari, W.W. Wits, The utilization of selective laser melting technology on heat transfer devices for thermal energy conversion applications: A review, *Renew. Sustain. Energy Rev.* (2018), doi: [10.1016/j.rser.2018.03.109](https://doi.org/10.1016/j.rser.2018.03.109).
- [14] L. Ventola, F. Robotti, M. Dialameh, F. Calignano, D. Manfredi, E. Chiavazzo, P. Asinari, Rough surfaces with enhanced heat transfer for electronics cooling by direct metal laser sintering, *Int. J. Heat Mass Transf.* (2014), doi: [10.1016/j.ijheatmasstransfer.2014.03.037](https://doi.org/10.1016/j.ijheatmasstransfer.2014.03.037).
- [15] C.K. Stimpson, J.C. Snyder, K.A. Thole, D. Mongillo, Roughness effects on flow and heat transfer for additively manufactured channels, *J. Turbomach.* (2016), doi: [10.1115/1.4032167](https://doi.org/10.1115/1.4032167).
- [16] C.K. Stimpson, J.C. Snyder, K.A. Thole, D. Mongillo, Scaling roughness effects on pressure loss and heat transfer of additively manufactured channels, *J. Turbomach.* (2017), doi: [10.1115/1.4034555](https://doi.org/10.1115/1.4034555).
- [17] J.C. Snyder, C.K. Stimpson, K.A. Thole, D. Mongillo, Build direction effects on additively manufactured channels, *J. Turbomach.* 138 (2016) 1–8, doi: [10.1115/1.4032168](https://doi.org/10.1115/1.4032168).
- [18] F. Calignano, D. Manfredi, E.P. Ambrosio, L. Iuliano, P. Fino, Influence of process parameters on surface roughness of aluminum parts produced by DMLS, *Int. J. Adv. Manuf. Technol.* (2013), doi: [10.1007/s00170-012-4688-9](https://doi.org/10.1007/s00170-012-4688-9).
- [19] M. Mohammadi, H. Asgari, Achieving low surface roughness AlSi10Mg_200C parts using direct metal laser sintering, *Addit. Manuf.* (2018), doi: [10.1016/j.addma.2017.12.012](https://doi.org/10.1016/j.addma.2017.12.012).
- [20] J. Delgado, J. Ciurana, C.A. Rodríguez, Influence of process parameters on part quality and mechanical properties for DMLS and SLM with iron-based materials, *Int. J. Adv. Manuf. Technol.* (2012), doi: [10.1007/s00170-011-3643-5](https://doi.org/10.1007/s00170-011-3643-5).
- [21] M. Launhardt, A. Wörz, A. Loderer, T. Laumer, D. Drummer, T. Hausotte, M. Schmidt, Detecting surface roughness on SLS parts with various measuring techniques, *Polym. Test.* (2016), doi: [10.1016/j.polymertesting.2016.05.022](https://doi.org/10.1016/j.polymertesting.2016.05.022).
- [22] A. Majeed, A. Ahmed, A. Salam, M.Z. Sheikh, Surface quality improvement by parameters analysis, optimization and heat treatment of AlSi10Mg parts manufactured by SLM additive manufacturing, *Int. J. Light. Mater. Manuf.* (2019), doi: [10.1016/j.jilmm.2019.08.001](https://doi.org/10.1016/j.jilmm.2019.08.001).
- [23] S.A. Shanmugasundaram, J. Razmi, M.J. Mian, L. Ladani, Mechanical anisotropy and surface roughness in additively manufactured parts fabricated by stereolithography (SLA) using statistical analysis, *Materials (Basel)*, 2020, doi: [10.3390/ma1312496](https://doi.org/10.3390/ma1312496).
- [24] Q. Lian, W. Sui, X. Wu, F. Yang, S. Yang, Additive manufacturing of ZrO₂ ceramic dental bridges by stereolithography, *Rapid Prototyp. J.* (2018), doi: [10.1108/RPJ-09-2016-0144](https://doi.org/10.1108/RPJ-09-2016-0144).
- [25] B. Agostini, M. Fabbrì, J.E. Park, L. Wojtan, J.R. Thome, B. Michel, State of the art of high heat flux cooling technologies, *Heat Transf. Eng.* (2007), doi: [10.1080/01457630601117799](https://doi.org/10.1080/01457630601117799).
- [26] T. Dixit, I. Ghosh, Review of micro- and mini-channel heat sinks and heat exchangers for single phase fluids, *Renew. Sustain. Energy Rev.* (2015), doi: [10.1016/j.rser.2014.09.024](https://doi.org/10.1016/j.rser.2014.09.024).
- [27] S.G. Kandlikar, W.J. Grande, Evolution of microchannel flow passages-thermohydraulic performance and fabrication technology, *Heat Transf. Eng.* (2003), doi: [10.1080/01457630304040](https://doi.org/10.1080/01457630304040).
- [28] M.A. Arie, A.H. Shooshtari, V.V. Rao, S.V. Dessiatoun, M.M. Ohadi, Air-Side Heat Transfer Enhancement Utilizing Design Optimization and an Additive Manufacturing Technique, *J. Heat Transfer.* (2017) 139, doi: [10.1115/1.4035068](https://doi.org/10.1115/1.4035068).
- [29] M.A. Arie, A. Shooshtari, M. Ohadi, Air side enhancement of heat transfer in an additively manufactured 1 kW heat exchanger for dry cooling applications, (2017) 1–8, <https://doi.org/10.1109/itherm.2017.8023956>.
- [30] M.A. Arie, A.H. Shooshtari, M.M. Ohadi, Experimental characterization of an additively manufactured heat exchanger for dry cooling of power plants, *Appl. Therm. Eng.* 129 (2018) 187–198, doi: [10.1016/j.applthermaleng.2017.09.140](https://doi.org/10.1016/j.applthermaleng.2017.09.140).
- [31] X. Zhang, R. Tiwari, A.H. Shooshtari, M.M. Ohadi, An additively manufactured metallic manifold-microchannel heat exchanger for high temperature applications, *Appl. Therm. Eng.* 143 (2018) 899–908, doi: [10.1016/j.applthermaleng.2018.08.032](https://doi.org/10.1016/j.applthermaleng.2018.08.032).
- [32] I.L. Collins, J.A. Weibel, L. Pan, S.V. Garimella, Evaluation of additively manufactured microchannel heat sinks, *IEEE Trans. Components, Packag. Manuf. Technol.* 9 (2019) 446–457, doi: [10.1109/TCMT.2018.2866972](https://doi.org/10.1109/TCMT.2018.2866972).
- [33] K.L. Kirsch, K.A. Thole, Experimental investigation of numerically optimized wavy microchannels created through additive manufacturing, *J. Turbomach.* (2018) 140, doi: [10.1115/1.4038180](https://doi.org/10.1115/1.4038180).
- [34] K.L. Kirsch, K.A. Thole, Numerical optimization, characterization, and experimental investigation of additively manufactured communicating microchannels, *J. Turbomach.* (2018) 140, doi: [10.1115/1.4041494](https://doi.org/10.1115/1.4041494).
- [35] K.L. Kirsch, K.A. Thole, Heat transfer and pressure loss measurements in additively manufactured wavy microchannels, *J. Turbomach.* (2017) 139, doi: [10.1115/1.4034342](https://doi.org/10.1115/1.4034342).
- [36] K.L. Kirsch, K.A. Thole, Isolating the effects of surface roughness versus wall shape in numerically optimized, additively manufactured micro cooling channels, *Exp. Therm. Fluid Sci.* 98 (2018) 227–238, doi: [10.1016/j.expthermflusci.2018.05.030](https://doi.org/10.1016/j.expthermflusci.2018.05.030).
- [37] I.L. Collins, J.A. Weibel, L. Pan, S.V. Garimella, A permeable-membrane microchannel heat sink made by additive manufacturing, *Int. J. Heat Mass Transf.* 131 (2019) 1174–1183, doi: [10.1016/j.ijheatmasstransfer.2018.11.126](https://doi.org/10.1016/j.ijheatmasstransfer.2018.11.126).
- [38] I. Kaur, P. Singh, Flow and Thermal Transport Through Unit Cell Topologies of Cubic and Octahedron Families, *Int. J. Heat Mass Transf.* (2020), doi: [10.1016/j.ijheatmasstransfer.2020.119784](https://doi.org/10.1016/j.ijheatmasstransfer.2020.119784).
- [39] M. Alsulami, M. Mortazavi, S.A. Niknam, D. Li, Design complexity and performance analysis in additively manufactured heat exchangers, *Int. J. Adv. Manuf. Technol.* 110 (2020) 865–873, doi: [10.1007/s00170-020-05898-3](https://doi.org/10.1007/s00170-020-05898-3).
- [40] W.C. Yameen, N.A. Piascik, A.K. Miller, R.C. Clemente, J.Z. Benner, A.D. Santamaria, S.A. Niknam, M. Mortazavi, Modified manifold-microchannel heat exchangers fabricated based on additive manufacturing: Experimental characterization, *ASME 2019 Heat Transf. Summer Conf. HT 2019*, Collocated with ASME 2019 13th Int. Conf. Energy Sustain., 2019, doi: [10.1115/HT2019-3535](https://doi.org/10.1115/HT2019-3535).
- [41] R. Tiwari, R.S. Andhare, A. Shooshtari, M. Ohadi, Development of an additive manufacturing-enabled compact manifold microchannel heat exchanger, *Appl. Therm. Eng.* 147 (2019) 781–788, doi: [10.1016/j.applthermaleng.2018.10.122](https://doi.org/10.1016/j.applthermaleng.2018.10.122).
- [42] H. Keramati, F. Battaglia, M.A. Arie, F. Singer, M.M. Ohadi, Additive manufacturing of compact manifold-microchannel heat exchangers utilizing direct metal laser sintering, in: *Intersoc. Conf. Therm. Thermomechanical Phenom. Electron. Syst. ITHERM. 2019–May*, 2019, pp. 423–429, doi: [10.1109/ITHERM.2019.8757447](https://doi.org/10.1109/ITHERM.2019.8757447).
- [43] S.S. Panse, S.V. Ekkad, Evaluation of Additively Manufactured Single-Pass and Two-Pass Enhanced Microchannel Heat Sinks, in: *Intersoc. Conf. Therm. Thermomechanical Phenom. Electron. Syst. ITHERM. 2020–July*, 2020, pp. 38–47, doi: [10.1109/ITHERM45881.2020.9190581](https://doi.org/10.1109/ITHERM45881.2020.9190581).
- [44] S.N. Joshi, Z. Yu, H. Sennouni, J. Hampshire, E.M. Dede, Single-phase Cooling Performance of a Topology Optimized and Additively-Manufactured Multi-Pass Branching Microchannel Heat Sink, in: *Intersoc. Conf. Therm. Thermomechanical Phenom. Electron. Syst. ITHERM. 2020–July*, 2020, pp. 790–795, doi: [10.1109/ITHERM45881.2020.9190597](https://doi.org/10.1109/ITHERM45881.2020.9190597).
- [45] H. Rastan, A. Abdi, B. Hamawandi, M. Ignatowicz, J.P. Meyer, B. Palm, Heat transfer study of enhanced additively manufactured minichannel heat exchangers, *Int. J. Heat Mass Transf.* (2020) 161, doi: [10.1016/j.ijheatmasstransfer.2020.120271](https://doi.org/10.1016/j.ijheatmasstransfer.2020.120271).
- [46] K. Huang, J.W. Wan, C.X. Chen, D.F. Mao, Y.Q. Li, Experiments investigation of the effects of surface roughness on laminar flow in macro tubes, *Exp. Therm. Fluid Sci.* 45 (2013) 243–248, doi: [10.1016/j.expthermflusci.2012.10.022](https://doi.org/10.1016/j.expthermflusci.2012.10.022).

- [47] S.G. Kandlikar, D. Schmitt, A.L. Carrano, J.B. Taylor, Characterization of surface roughness effects on pressure drop in single-phase flow in minichannels, *Phys. Fluids.* 17 (2005), doi: [10.1063/1.1896985](https://doi.org/10.1063/1.1896985).
- [48] B. Dai, M. Li, Y. Ma, Effect of surface roughness on liquid friction and transition characteristics in micro- and mini-channels, *Appl. Therm. Eng.* 67 (2014) 283–293, doi: [10.1016/j.applthermaleng.2014.03.028](https://doi.org/10.1016/j.applthermaleng.2014.03.028).
- [49] J.C. Han, Heat transfer and friction characteristics in rectangular channels with rib tabulators, *J. Heat Transfer.* (1988), doi: [10.1115/1.3250487](https://doi.org/10.1115/1.3250487).
- [50] J.S. Park, J.C. Han, Y. Huang, S. Ou, R.J. Boyle, Heat transfer performance comparisons of five different rectangular channels with parallel angled ribs, *Int. J. Heat Mass Transf.* (1992), doi: [10.1016/0017-9310\(92\)90309-G](https://doi.org/10.1016/0017-9310(92)90309-G).
- [51] Y. Rao, B. Li, Y. Feng, Heat transfer of turbulent flow over surfaces with spherical dimples and teardrop dimples, *Exp. Therm. Fluid Sci.* (2015), doi: [10.1016/j.expthermflusci.2014.10.030](https://doi.org/10.1016/j.expthermflusci.2014.10.030).
- [52] S.W. Moon, S.C. Lau, Turbulent heat transfer measurements on a wall with concave and cylindrical dimples in a square channel, *Am. Soc. Mech. Eng. Int. Gas Turbine Institute, Turbo Expo IGTI.* 2002, doi: [10.1115/GT2002-30208](https://doi.org/10.1115/GT2002-30208).
- [53] M.K. Chyu, Y. Yu, H. Ding, J.P. Downs, F.O. Soeckting, Concavity enhanced heat transfer in an internal cooling passag, in: *Proc. ASME Turbo Expo*, 1997, doi: [10.1115/97-GT-437](https://doi.org/10.1115/97-GT-437).
- [54] N.K. Burgess, P.M. Ligrani, Effects of dimple depth on channel nusselt numbers and friction factors, *J. Heat Transfer.* (2005), doi: [10.1115/1.1994880](https://doi.org/10.1115/1.1994880).
- [55] K. Saha, S. Acharya, Heat transfer enhancement using angled grooves as turbulence promoters, *J. Turbomach.* (2014), doi: [10.1115/1.4025733](https://doi.org/10.1115/1.4025733).
- [56] M.K. Chyu, Y.C. Hsing, V. Natarajan, Convective heat transfer of cubic fin arrays in a narrow channel, *J. Turbomach.* (1998), doi: [10.1115/1.2841414](https://doi.org/10.1115/1.2841414).
- [57] K.L. Kirsch, K.A. Thole, Pressure loss and heat transfer performance for additively and conventionally manufactured pin fin arrays, *Int. J. Heat Mass Transf.* 108 (2017) 2502–2513, doi: [10.1016/j.ijheatmasstransfer.2017.01.095](https://doi.org/10.1016/j.ijheatmasstransfer.2017.01.095).
- [58] P.M. Ligrani, M.M. Oliveira, T. Blaskovich, Comparison of heat transfer augmentation techniques, *AIAA J.* (2003), doi: [10.2514/2.1964](https://doi.org/10.2514/2.1964).
- [59] K.K. Ferster, K.L. Kirsch, K.A. Thole, Effects of geometry, spacing, and number of pin fins in additively manufactured microchannel pin fin arrays, *J. Turbomach.* 140 (2018) 1–10, doi: [10.1115/1.4038179](https://doi.org/10.1115/1.4038179).
- [60] Y. Cormier, P. Dupuis, A. Farjam, A. Corbeil, B. Jodoin, Additive manufacturing of pyramidal pin fins: Height and fin density effects under forced convection, *Int. J. Heat Mass Transf.* (2014), doi: [10.1016/j.ijheatmasstransfer.2014.03.053](https://doi.org/10.1016/j.ijheatmasstransfer.2014.03.053).
- [61] P. Dupuis, Y. Cormier, M. Fenech, A. Corbeil, B. Jodoin, Flow structure identification and analysis in fin arrays produced by cold spray additive manufacturing, *Int. J. Heat Mass Transf.* 93 (2016) 301–313, doi: [10.1016/j.ijheatmasstransfer.2015.10.019](https://doi.org/10.1016/j.ijheatmasstransfer.2015.10.019).
- [62] A. Farjam, Y. Cormier, P. Dupuis, B. Jodoin, A. Corbeil, Influence of Alumina Addition to Aluminum Fins for Compact Heat Exchangers Produced by Cold Spray Additive Manufacturing, *J. Therm. Spray Technol.* (2015), doi: [10.1007/s11666-015-0305-4](https://doi.org/10.1007/s11666-015-0305-4).
- [63] P. Dupuis, Y. Cormier, M. Fenech, B. Jodoin, Heat transfer and flow structure characterization for pin fins produced by cold spray additive manufacturing, *Int. J. Heat Mass Transf.* (2016), doi: [10.1016/j.ijheatmasstransfer.2016.03.069](https://doi.org/10.1016/j.ijheatmasstransfer.2016.03.069).
- [64] B. Kwon, L. Liebenberg, A.M. Jacobi, W.P. King, Heat transfer enhancement of internal laminar flows using additively manufactured static mixers, *Int. J. Heat Mass Transf.* 137 (2019) 292–300, doi: [10.1016/j.ijheatmasstransfer.2019.03.133](https://doi.org/10.1016/j.ijheatmasstransfer.2019.03.133).
- [65] M. Searle, J. Black, D. Straub, E. Robey, J. Yip, S. Ramesh, A. Roy, A.S. Sabau, D. Molot, Heat transfer coefficients of additively manufactured tubes with internal pin fins for supercritical carbon dioxide cycle recuperators, *Appl. Therm. Eng.* 181 (2020) 116030, doi: [10.1016/j.applthermaleng.2020.116030](https://doi.org/10.1016/j.applthermaleng.2020.116030).
- [66] S. Unger, M. Beyer, S. Gruber, R. Willner, U. Hampel, Experimental study on the air-side thermal-flow performance of additively manufactured heat exchangers with novel fin designs, *Int. J. Therm. Sci.* 146 (2019) 106074, doi: [10.1016/j.ijthermalsci.2019.106074](https://doi.org/10.1016/j.ijthermalsci.2019.106074).
- [67] D. Saltzman, M. Bichnevicius, S. Lynch, T.W. Simpson, E.W. Reutzel, C. Dickman, R. Martukanitz, Design and evaluation of an additively manufactured aircraft heat exchanger, *Appl. Therm. Eng.* 138 (2018) 254–263, doi: [10.1016/j.applthermaleng.2018.04.032](https://doi.org/10.1016/j.applthermaleng.2018.04.032).
- [68] M. Bichnevicius, D. Saltzman, S. Lynch, Comparison of Additively Manufactured Louvered Plate-Fin Heat Exchangers, *J. Therm. Sci. Eng. Appl.* 12 (2020), doi: [10.1115/1.4044348](https://doi.org/10.1115/1.4044348).
- [69] D. Saltzman, M. Bichnevicius, S. Lynch, T.W. Simpson, E.W. Reutzel, C. Dickman, R. Martukanitz, Experimental comparison of a traditionally built versus additively manufactured aircraft heat exchanger, *AIAA SciTech Forum - 55th AIAA Aerosp. Sci. Meet.* (2017), doi: [10.2514/6.2017-0902](https://doi.org/10.2514/6.2017-0902).
- [70] C.Y. Zhao, Review on thermal transport in high porosity cellular metal foams with open cells, *Int. J. Heat Mass Transf.* (2012), doi: [10.1016/j.ijheatmasstransfer.2012.03.017](https://doi.org/10.1016/j.ijheatmasstransfer.2012.03.017).
- [71] V.S. Deshpande, N.A. Fleck, M.F. Ashby, Effective properties of the octet-truss lattice material, *J. Mech. Phys. Solids.* (2001), doi: [10.1016/S0022-5096\(01\)00010-2](https://doi.org/10.1016/S0022-5096(01)00010-2).
- [72] A. Chaudhari, P. Ekade, S. Krishnan, Experimental investigation of heat transfer and fluid flow in octet-truss lattice geometry, *Int. J. Therm. Sci.* (2019), doi: [10.1016/j.ijthermalsci.2019.05.003](https://doi.org/10.1016/j.ijthermalsci.2019.05.003).
- [73] P. Ekade, S. Krishnan, Fluid flow and heat transfer characteristics of octet truss lattice geometry, *Int. J. Therm. Sci.* (2019), doi: [10.1016/j.ijthermalsci.2018.11.031](https://doi.org/10.1016/j.ijthermalsci.2018.11.031).
- [74] K.K. Wong, K.C. Leong, Saturated pool boiling enhancement using porous lattice structures produced by Selective Laser Melting, *Int. J. Heat Mass Transf.* (2018), doi: [10.1016/j.ijheatmasstransfer.2017.12.148](https://doi.org/10.1016/j.ijheatmasstransfer.2017.12.148).
- [75] J.Y. Ho, K.K. Wong, K.C. Leong, Saturated pool boiling of FC-72 from enhanced surfaces produced by Selective Laser Melting, *Int. J. Heat Mass Transf.* (2016), doi: [10.1016/j.ijheatmasstransfer.2016.03.073](https://doi.org/10.1016/j.ijheatmasstransfer.2016.03.073).
- [76] J.Y. Ho, K.K. Wong, K.C. Leong, C. Yang, Enhanced nucleate pool boiling from microstructured surfaces fabricated by selective laser melting, in: *ASME 2016 5th Int. Conf. Micro/Nanoscale Heat Mass Transf. MNHMT, 2016*, p. 2016, doi: [10.1115/MNHMT2016-6616](https://doi.org/10.1115/MNHMT2016-6616).
- [77] R.J. MacNamara, T.L. Lupton, R. Lupoi, A.J. Robinson, Enhanced nucleate pool boiling on copper-diamond textured surfaces, *Appl. Therm. Eng.* (2019), doi: [10.1016/j.applthermaleng.2019.114145](https://doi.org/10.1016/j.applthermaleng.2019.114145).
- [78] X.W. Wang, J.Y. Ho, K.C. Leong, An experimental investigation of single droplet impact cooling on hot enhanced surfaces fabricated by selective laser melting, *Int. J. Heat Mass Transf.* (2018), doi: [10.1016/j.ijheatmasstransfer.2017.12.033](https://doi.org/10.1016/j.ijheatmasstransfer.2017.12.033).
- [79] J.Y. Ho, K.C. Leong, T.N. Wong, Experimental and numerical investigation of forced convection heat transfer in porous lattice structures produced by selective laser melting, *Int. J. Therm. Sci.* (2019), doi: [10.1016/j.ijthermalsci.2018.11.022](https://doi.org/10.1016/j.ijthermalsci.2018.11.022).
- [80] J.Y. Ho, K.C. Leong, Cylindrical porous inserts for enhancing the thermal and hydraulic performance of water-cooled cold plates, *Appl. Therm. Eng.* (2017), doi: [10.1016/j.applthermaleng.2017.04.101](https://doi.org/10.1016/j.applthermaleng.2017.04.101).
- [81] J.Y. Ho, K.C. Leong, T.N. Wong, Additively-manufactured metallic porous lattice heat exchangers for air-side heat transfer enhancement, *Int. J. Heat Mass Transf.* (2020), doi: [10.1016/j.ijheatmasstransfer.2019.119262](https://doi.org/10.1016/j.ijheatmasstransfer.2019.119262).
- [82] D. Shamvedi, O.J. McCarthy, E. O'Donoghue, C. Danilenko, P. O'Leary, R. Raghavendra, 3D Metal printed heat sinks with longitudinally varying lattice structure sizes using direct metal laser sintering, *Virtual Phys. Prototyp.* (2018), doi: [10.1080/17452759.2018.1479528](https://doi.org/10.1080/17452759.2018.1479528).
- [83] J. Broughton, Y.K. Joshi, Comparison of single-phase convection in additive manufactured versus traditional metal foams, *J. Heat Transfer.* (2020), doi: [10.1115/1.4046972](https://doi.org/10.1115/1.4046972).
- [84] M. Wong, I. Owen, C.J. Sutcliffe, A. Puri, Convective heat transfer and pressure losses across novel heat sinks fabricated by Selective Laser Melting, *Int. J. Heat Mass Transf.* (2009), doi: [10.1016/j.ijheatmasstransfer.2008.06.002](https://doi.org/10.1016/j.ijheatmasstransfer.2008.06.002).
- [85] J.Y. Ho, K.K. Wong, K.C. Leong, T.N. Wong, Convective heat transfer performance of airfoil heat sinks fabricated by selective laser melting, *Int. J. Therm. Sci.* (2017), doi: [10.1016/j.ijthermalsci.2016.12.016](https://doi.org/10.1016/j.ijthermalsci.2016.12.016).
- [86] M. Klumpp, A. Inayat, J. Schwerdtfeger, C. Körner, R.F. Singer, H. Freund, W. Schwieger, Periodic open cellular structures with ideal cubic cell geometry: Effect of porosity and cell orientation on pressure drop behavior, *Chem. Eng. J.* (2014), doi: [10.1016/j.cej.2013.12.060](https://doi.org/10.1016/j.cej.2013.12.060).
- [87] D. Liang, W. Bai, W. Chen, M.K. Chyu, Investigating the effect of element shape of the face-centered cubic lattice structure on the flow and endwall heat transfer characteristics in a rectangular channel, *Int. J. Heat Mass Transf.* (2020), doi: [10.1016/j.ijheatmasstransfer.2020.119579](https://doi.org/10.1016/j.ijheatmasstransfer.2020.119579).
- [88] S. Yun, J. Kwon, D.C. Lee, H.H. Shin, Y. Kim, Heat transfer and stress characteristics of additive manufactured FCCZ lattice channel using thermal fluid-structure interaction model, *Int. J. Heat Mass Transf.* (2020), doi: [10.1016/j.ijheatmasstransfer.2019.119187](https://doi.org/10.1016/j.ijheatmasstransfer.2019.119187).
- [89] S. Parbat, Z. Min, L. Yang, M. Chyu, Experimental and numerical analysis of additively manufactured inconel 718 coupons with lattice structure, *J. Turbomach.* (2020), doi: [10.1115/1.4046527](https://doi.org/10.1115/1.4046527).
- [90] B. Shen, Y. Li, H. Yan, S.K.S. Boetcher, G. Xie, Heat transfer enhancement of wedge-shaped channels by replacing pin fins with Kagome lattice structures, *Int. J. Heat Mass Transf.* (2019), doi: [10.1016/j.ijheatmasstransfer.2019.06.059](https://doi.org/10.1016/j.ijheatmasstransfer.2019.06.059).
- [91] O. Al-Ketan, R.K. Abu Al-Rub, Multifunctional Mechanical Metamaterials Based on Triply Periodic Minimal Surface Lattices, *Adv. Eng. Mater.* (2019), doi: [10.1002/adem.201900524](https://doi.org/10.1002/adem.201900524).
- [92] J. Shi, L. Zhu, L. Li, Z. Li, J. Yang, X. Wang, A TPMS-based method for modeling porous scaffolds for bionic bone tissue engineering, *Sci. Rep.* (2018), doi: [10.1038/s41598-018-25750-9](https://doi.org/10.1038/s41598-018-25750-9).
- [93] O. Al-Ketan, D.W. Lee, R. Rowshan, R.K. Abu Al-Rub, Functionally graded and multi-morphology sheet TPMS lattices: Design, manufacturing, and mechanical properties, *J. Mech. Behav. Biomed. Mater.* (2020), doi: [10.1016/j.jmbbm.2019.103520](https://doi.org/10.1016/j.jmbbm.2019.103520).
- [94] S.C. Kapfer, S.T. Hyde, K. Mecke, C.H. Arns, G.E. Schröder-Turk, Minimal surface scaffold designs for tissue engineering, *Biomaterials* (2011), doi: [10.1016/j.biomaterials.2011.06.012](https://doi.org/10.1016/j.biomaterials.2011.06.012).
- [95] O. Al-Ketan, R. Rowshan, R.K. Abu Al-Rub, Topology-mechanical property relationship of 3D printed strut, skeletal, and sheet based periodic metallic cellular materials, *Addit. Manuf.* (2018), doi: [10.1016/j.addma.2017.12.006](https://doi.org/10.1016/j.addma.2017.12.006).
- [96] D.W. Abueidda, M. Elhebeary, C.S. (Andrew) Shiang, S. Pang, R.K. Abu Al-Rub, I.M. Jasius, Mechanical properties of 3D printed polymeric Gyroid cellular structures: Experimental and finite element study, *Mater. Des.* (2019), doi: [10.1016/j.matdes.2019.107597](https://doi.org/10.1016/j.matdes.2019.107597).
- [97] L. Yang, R. Mertens, M. Ferrucci, C. Yan, Y. Shi, S. Yang, Continuous graded Gyroid cellular structures fabricated by selective laser melting: Design, manufacturing and mechanical properties, *Mater. Des.* (2019), doi: [10.1016/j.matdes.2018.12.007](https://doi.org/10.1016/j.matdes.2018.12.007).
- [98] Y. Jung, S. Torquato, Fluid permeabilities of triply periodic minimal surfaces, *Phys. Rev. E - Stat. Nonlinear, Soft Matter Phys.* (2005), doi: [10.1103/PhysRevE.72.056319](https://doi.org/10.1103/PhysRevE.72.056319).
- [99] H. Montazerian, M.G.A. Mohamed, M.M. Montazeri, S. Kheiri, A.S. Milani, K. Kim, M. Hoorfar, Permeability and mechanical properties of gradient porous PDMS scaffolds fabricated by 3D-printed sacrificial templates designed with minimal surfaces, *Acta Biomater.* (2019), doi: [10.1016/j.actbio.2019.06.040](https://doi.org/10.1016/j.actbio.2019.06.040).

- [100] M. Zhanmanesh, M. Varmazyar, H. Montazerian, Fluid Permeability of Graded Porosity Scaffolds Architectured with Minimal Surfaces, *ACS Biomater. Sci. Eng.* (2019), doi: [10.1021/acsbiomaterials.8b01400](https://doi.org/10.1021/acsbiomaterials.8b01400).
- [101] H. Montazerian, E. Davoodi, M. Asadi-Eydivand, J. Kadkhodapour, M. Solati-Hashjin, Porous scaffold internal architecture design based on minimal surfaces: A compromise between permeability and elastic properties, *Mater. Des.* (2017), doi: [10.1016/j.matdes.2017.04.009](https://doi.org/10.1016/j.matdes.2017.04.009).
- [102] S. Ma, Q. Tang, X. Han, Q. Feng, J. Song, R. Setchi, Y. Liu, Y. Liu, A. Goulas, D.S. Engström, Y.Y. Tse, N. Zhen, Manufacturability, Mechanical Properties, Mass-Transport Properties and Biocompatibility of Triply Periodic Minimal Surface (TPMS) Porous Scaffolds Fabricated by Selective Laser Melting, *Mater. Des.* (2020), doi: [10.1016/j.matdes.2020.109034](https://doi.org/10.1016/j.matdes.2020.109034).
- [103] A.P.G. Castro, T. Pires, J.E. Santos, B.P. Gouveia, P.R. Fernandes, Permeability versus design in TPMS scaffolds, *Materials (Basel.)* (2019), doi: [10.3390/ma12081313](https://doi.org/10.3390/ma12081313).
- [104] S.B.G. Blanquer, M. Werner, M. Hannula, S. Sharifi, G.P.R. Lajoinie, D. Eglin, J. Hyttinen, A.A. Poot, D.W. Grijpma, Surface curvature in triply-periodic minimal surface architectures as a distinct design parameter in preparing advanced tissue engineering scaffolds, *Biofabrication* (2017), doi: [10.1088/1758-5090/aa6553](https://doi.org/10.1088/1758-5090/aa6553).
- [105] A. Arjunan, M. Demetriadou, A. Baroutaji, C. Wang, Mechanical performance of highly permeable laser melted Ti6Al4V bone scaffolds, *J. Mech. Behav. Biomed. Mater.* (2020), doi: [10.1016/j.jmbbm.2019.103517](https://doi.org/10.1016/j.jmbbm.2019.103517).
- [106] J. Santos, T. Pires, B.P. Gouveia, A.P.G. Castro, P.R. Fernandes, On the permeability of TPMS scaffolds, *J. Mech. Behav. Biomed. Mater.* (2020), doi: [10.1016/j.jmbbm.2020.103932](https://doi.org/10.1016/j.jmbbm.2020.103932).
- [107] H. Montazerian, M. Zhanmanesh, E. Davoodi, A.S. Milani, M. Hoofifar, Longitudinal and radial permeability analysis of additively manufactured porous scaffolds: Effect of pore shape and porosity, *Mater. Des.* (2017), doi: [10.1016/j.matdes.2017.03.006](https://doi.org/10.1016/j.matdes.2017.03.006).
- [108] D.W. Abueida, R.K. Abu Al-Rub, A.S. Dalaq, D.W. Lee, K.A. Khan, I. Jasiuk, Effective conductivities and elastic moduli of novel foams with triply periodic minimal surfaces, *Mech. Mater.* (2016), doi: [10.1016/j.mechmat.2016.01.004](https://doi.org/10.1016/j.mechmat.2016.01.004).
- [109] S. Catchpole-Smith, R.R.J. Sélo, A.W. Davis, I.A. Ashcroft, C.J. Tuck, A. Clare, Thermal conductivity of TPMS lattice structures manufactured via laser powder bed fusion, *Addit. Manuf.* (2019), doi: [10.1016/j.addma.2019.100846](https://doi.org/10.1016/j.addma.2019.100846).
- [110] A. Mirabolghasemi, A.H. Akbarzadeh, D. Rodrigue, D. Therriault, Thermal conductivity of architected cellular metamaterials, *Acta Mater.* (2019), doi: [10.1016/j.actamat.2019.04.061](https://doi.org/10.1016/j.actamat.2019.04.061).
- [111] R.R.J. Sélo, S. Catchpole-Smith, I. Maskery, I. Ashcroft, C. Tuck, On the thermal conductivity of AlSi10Mg and lattice structures made by laser powder bed fusion, *Addit. Manuf.* (2020), doi: [10.1016/j.addma.2020.101214](https://doi.org/10.1016/j.addma.2020.101214).
- [112] O. Al-Ketan, M. Ali, M. Khalil, R. Rowshan, K.A. Khan, R.K. Abu Al-Rub, Forced Convection Computational Fluid Dynamics Analysis of Architected and Three-Dimensional Printable Heat Sinks Based on Triply Periodic Minimal Surfaces, *J. Therm. Sci. Eng. Appl.* (2021), doi: [10.1115/1.4047385](https://doi.org/10.1115/1.4047385).
- [113] C. Huang, W. Cai, Y. Wang, Y. Liu, Q. Li, B. Li, Review on the characteristics of flow and heat transfer in printed circuit heat exchangers, *Appl. Therm. Eng.* 153 (2019) 190–205, doi: [10.1016/j.aplthermaleng.2019.02.131](https://doi.org/10.1016/j.aplthermaleng.2019.02.131).
- [114] N. Tsuzuki, Y. Kato, T. Ishiduka, High performance printed circuit heat exchanger, *Appl. Therm. Eng.* 27 (2007) 1702–1707, doi: [10.1016/j.aplthermaleng.2006.07.007](https://doi.org/10.1016/j.aplthermaleng.2006.07.007).
- [115] W. Li, G. Yu, Z. Yu, Bioinspired heat exchangers based on triply periodic minimal surfaces for supercritical CO₂ cycles, *Appl. Therm. Eng.* (2020), doi: [10.1016/j.aplthermaleng.2020.115686](https://doi.org/10.1016/j.aplthermaleng.2020.115686).
- [116] J. Kim, D.-J. Yoo, 3D printed compact heat exchangers with mathematically defined core structures, *J. Comput. Des. Eng.* (2020), doi: [10.1093/jcde/qwaa032](https://doi.org/10.1093/jcde/qwaa032).
- [117] I. Echeta, X. Feng, B. Dutton, R. Leach, S. Piano, Review of defects in lattice structures manufactured by powder bed fusion, *Int. J. Adv. Manuf. Technol.* (2020), doi: [10.1007/s00170-019-04753-4](https://doi.org/10.1007/s00170-019-04753-4).
- [118] A.D. Dressler, E.W. Jost, J.C. Miers, D.G. Moore, C.C. Seepersad, B.L. Boyce, Heterogeneities dominate mechanical performance of additively manufactured metal lattice struts, *Addit. Manuf.* (2019), doi: [10.1016/j.addma.2019.06.011](https://doi.org/10.1016/j.addma.2019.06.011).
- [119] N. Thomas, N. Sreedhar, O. Al-Ketan, R. Rowshan, R.K. Abu Al-Rub, H. Arafat, 3D printed spacers based on TPMS architectures for scaling control in membrane distillation, *J. Membr. Sci.* (2019), doi: [10.1016/j.memsci.2019.03.039](https://doi.org/10.1016/j.memsci.2019.03.039).
- [120] E.H.C. Castillo, N. Thomas, O. Al-Ketan, R. Rowshan, R.K. Abu Al-Rub, L.D. Nghiem, S. Vigneswaran, H.A. Arafat, G. Naidu, 3D printed spacers for organic fouling mitigation in membrane distillation, *J. Membr. Sci.* (2019), doi: [10.1016/j.memsci.2019.03.040](https://doi.org/10.1016/j.memsci.2019.03.040).
- [121] N. Sreedhar, N. Thomas, O. Al-Ketan, R. Rowshan, H.H. Hernandez, R.K. Abu Al-Rub, H.A. Arafat, Mass transfer analysis of ultrafiltration using spacers based on triply periodic minimal surfaces: Effects of spacer design, directionality and voidage, *J. Membr. Sci.* (2018), doi: [10.1016/j.memsci.2018.05.028](https://doi.org/10.1016/j.memsci.2018.05.028).
- [122] M. Ouda, O. Al-Ketan, N. Sreedhar, M.I. Hasan Ali, R.K. Abu Al-Rub, S. Hong, H.A. Arafat, Novel static mixers based on triply periodic minimal surface (TPMS) architectures, *J. Environ. Chem. Eng.* (2020), doi: [10.1016/j.jece.2020.104289](https://doi.org/10.1016/j.jece.2020.104289).
- [123] H. Ye, R. Sokolovskij, H.W. Van Zeijl, A.W.J. Gielen, G. Zhang, A polymer based miniature loop heat pipe with silicon substrate and temperature sensors for high brightness light-emitting diodes, *Microelectron. Reliab.* (2014), doi: [10.1016/j.microrel.2014.02.032](https://doi.org/10.1016/j.microrel.2014.02.032).
- [124] H. Wang, J. Qu, Q. Sun, Z. Kang, X. Han, Thermal characteristic comparison of three-dimensional oscillating heat pipes with/without sintered copper particles inside flat-plate evaporator for concentrating photovoltaic cooling, *Appl. Therm. Eng.* (2020), doi: [10.1016/j.aplthermaleng.2019.114815](https://doi.org/10.1016/j.aplthermaleng.2019.114815).
- [125] Q. Su, S. Chang, Y. Zhao, H. Zheng, C. Dang, A review of loop heat pipes for aircraft anti-icing applications, *Appl. Therm. Eng.* (2018), doi: [10.1016/j.aplthermaleng.2017.11.030](https://doi.org/10.1016/j.aplthermaleng.2017.11.030).
- [126] C. Wang, J. Chen, S. Qiu, W. Tian, D. Zhang, G.H. Su, Performance analysis of heat pipe radiator unit for space nuclear power reactor, *Ann. Nucl. Energy.* (2017), doi: [10.1016/j.anucene.2017.01.015](https://doi.org/10.1016/j.anucene.2017.01.015).
- [127] V.G. Pastukhov, Y.F. Maidanik, C.V. Vershinin, M.A. Korukov, Miniature loop heat pipes for electronics cooling, *Appl. Therm. Eng.* (2003), doi: [10.1016/S1359-4311\(03\)00046-2](https://doi.org/10.1016/S1359-4311(03)00046-2).
- [128] A. Faghri, Review and advances in heat pipe science and technology, *J. Heat Transfer.* (2012), doi: [10.1115/1.4007407](https://doi.org/10.1115/1.4007407).
- [129] X. Chen, H. Ye, X. Fan, T. Ren, G. Zhang, A review of small heat pipes for electronics, *Appl. Therm. Eng.* (2016), doi: [10.1016/j.aplthermaleng.2015.11.048](https://doi.org/10.1016/j.aplthermaleng.2015.11.048).
- [130] C.B. Sobhan, R.L. Rag, G.P. Peterson, A review and comparative study of the investigations on micro heat pipes, *Int. J. Energy Res.* (2007), doi: [10.1002/er.1285](https://doi.org/10.1002/er.1285).
- [131] R. Savino, A. Cecere, R. Di Paola, Surface tension-driven flow in wickless heat pipes with self-rewetting fluids, *Int. J. Heat Fluid Flow.* (2009), doi: [10.1016/j.ijheatfluidflow.2009.01.009](https://doi.org/10.1016/j.ijheatfluidflow.2009.01.009).
- [132] V.V. Calmidi, R.L. Mahajan, The effective thermal conductivity of high porosity fibrous metal foams, *J. Heat Transfer.* (1999), doi: [10.1115/1.2826001](https://doi.org/10.1115/1.2826001).
- [133] R. Wulf, M.A.A. Mendes, V. Skibina, A. Al-Zoubi, D. Trimis, S. Ray, U. Gross, Experimental and numerical determination of effective thermal conductivity of open cell FeCrAl-alloy metal foams, *Int. J. Therm. Sci.* (2014), doi: [10.1016/j.ijthermalsci.2014.06.030](https://doi.org/10.1016/j.ijthermalsci.2014.06.030).
- [134] D. Jafari, W.W. Wits, B.J. Geurts, Metal 3D-printed wick structures for heat pipe application: Capillary performance analysis, *Appl. Therm. Eng.* (2018), doi: [10.1016/j.aplthermaleng.2018.07.111](https://doi.org/10.1016/j.aplthermaleng.2018.07.111).
- [135] M.J. Rightley, C.P. Tigges, R.C. Givler, C.V. Robino, J.J. Mulhall, P.M. Smith, Innovative wick design for multi-source, flat plate heat pipes, *Microelectronics J.* (2003), doi: [10.1016/S0026-2692\(02\)00187-8](https://doi.org/10.1016/S0026-2692(02)00187-8).
- [136] T. Yong, C. Ping, W. Xiaowu, Experimental investigation into the performance of heat pipe with micro grooves fabricated by Extrusion-ploughing process, *Energy Convers. Manag.* (2010), doi: [10.1016/j.enconman.2010.01.001](https://doi.org/10.1016/j.enconman.2010.01.001).
- [137] A. Faghri, HEAT PIPE: REVIEW, OPPORTUNITIES AND CHALLENGES, *Front. Heat Pipes.* (2014), doi: [10.5098/fhp.5.1](https://doi.org/10.5098/fhp.5.1).
- [138] M. Ameli, B. Agnew, P.S. Leung, B. Ng, C.J. Sutcliffe, J. Singh, R. McGlen, A novel method for manufacturing sintered aluminium heat pipes (SAHP), *Appl. Therm. Eng.* (2013), doi: [10.1016/j.aplthermaleng.2012.12.011](https://doi.org/10.1016/j.aplthermaleng.2012.12.011).
- [139] J. Esarte, J.M. Blanco, A. Bernardini, J.T. San-José, Optimizing the design of a two-phase cooling system loop heat pipe: Wick manufacturing with the 3D selective laser melting printing technique and prototype testing, *Appl. Therm. Eng.* (2017), doi: [10.1016/j.aplthermaleng.2016.09.123](https://doi.org/10.1016/j.aplthermaleng.2016.09.123).
- [140] O.T. Ibrahim, J.G. Monroe, S.M. Thompson, N. Shamsaei, H. Bilheux, A. Elwany, L. Bian, An investigation of a multi-layered oscillating heat pipe additively manufactured from Ti-6Al-4V powder, *Int. J. Heat Mass Transf.* 108 (2017) 1036–1047, doi: [10.1016/j.ijheatmasstransfer.2016.12.063](https://doi.org/10.1016/j.ijheatmasstransfer.2016.12.063).
- [141] S.M. Thompson, Z.S. Aspin, N. Shamsaei, A. Elwany, L. Bian, Additive manufacturing of heat exchangers: A case study on a multi-layered Ti-6Al-4V oscillating heat pipe, *Addit. Manuf.* 8 (2015) 163–174, doi: [10.1016/j.addma.2015.09.003](https://doi.org/10.1016/j.addma.2015.09.003).
- [142] D. Jafari, W.W. Wits, B.J. Geurts, Phase change heat transfer characteristics of an additively manufactured wick for heat pipe applications, *Appl. Therm. Eng.* 168 (2020) 114890, doi: [10.1016/j.aplthermaleng.2019.114890](https://doi.org/10.1016/j.aplthermaleng.2019.114890).
- [143] D. Jafari, W.W. Wits, B. Jgeurts, An investigation of porous structure characteristics of heat pipes made by additive manufacturing, *THERMINIC 2017 - 23rd Int. Work. Therm. Investig. ICs Syst.*, 2017, doi: [10.1109/THERMINIC.2017.8233841](https://doi.org/10.1109/THERMINIC.2017.8233841).
- [144] R.S. Bunker, A review of shaped hole turbine film-cooling technology, *J. Heat Transfer.* (2005), doi: [10.1115/1.1860562](https://doi.org/10.1115/1.1860562).
- [145] R.S. Bunker, The effects of manufacturing tolerances on gas turbine cooling, *J. Turbomach.* (2009), doi: [10.1115/1.3072494](https://doi.org/10.1115/1.3072494).
- [146] R.P. Schroeder, K.A. Thole, Effect of in-hole roughness on film cooling from a shaped hole, *J. Turbomach.* (2017), doi: [10.1115/1.4034847](https://doi.org/10.1115/1.4034847).
- [147] M. Srinivas, B.S. Babu, A Critical Review on Recent Research Methodologies in Additive Manufacturing, *Mater. Today Proc.* (2017) 9049–9059, doi: [10.1016/j.mtpr.2017.07.258](https://doi.org/10.1016/j.mtpr.2017.07.258).
- [148] L. Di Angelo, P. Di Stefano, E. Guardiani, Search for the optimal build direction in additive manufacturing technologies: A review, *J. Manuf. Mater. Process.* 4 (2020), doi: [10.3390/JMMP4030071](https://doi.org/10.3390/JMMP4030071).
- [149] J.C. Snyder, C.K. Stimpson, K.A. Thole, D.J. Mongillo, Build Direction Effects on Microchannel Tolerance and Surface Roughness, *J. Mech. Des. Trans. ASME.* 137 (2015), doi: [10.1115/1.4031071](https://doi.org/10.1115/1.4031071).
- [150] R.I. Campbell, M. Martorelli, H.S. Lee, Surface roughness visualisation for rapid prototyping models, *CAD Comput. Aided Des.* 34 (2002) 717–725, doi: [10.1016/S0010-4485\(01\)00201-9](https://doi.org/10.1016/S0010-4485(01)00201-9).
- [151] C.K. Stimpson, J.C. Snyder, K.A. Thole, D. Mongillo, Effectiveness measurements of additively manufactured film cooling holes, *J. Turbomach.* (2018), doi: [10.1115/1.4038182](https://doi.org/10.1115/1.4038182).
- [152] C.K. Stimpson, J.C. Snyder, K.A. Thole, D. Mongillo, Effects of coolant feed direction on additively manufactured film cooling holes, *J. Turbomach.* (2018), doi: [10.1115/1.4041374](https://doi.org/10.1115/1.4041374).

- [153] J.C. Snyder, K.A. Thole, Performance of public film cooling geometries produced through additive manufacturing, *J. Turbomach.* (2020), doi:10.1115/1.4046488.
- [154] J.C. Snyder, K.A. Thole, Effect of additive manufacturing process parameters on turbine cooling, *J. Turbomach.* (2020), doi:10.1115/1.4046459.
- [155] K.L. Kirsch, J.C. Snyder, C.K. Stimpson, K.A. Thole, D. Mongillo, Repeatability in performance of micro cooling geometries manufactured with laser powder bed fusion, in: 53rd AIAA/SAE/ASEE Jt. Propuls. Conf., 2017, p. 2017, doi:10.2514/6.2017-4706.
- [156] J. Snyder, K. Thole, Tailoring Surface Roughness Using Additive Manufacturing to Improve Internal Cooling, *J. Turbomach.* (2020), doi:10.1115/1.4047380.
- [157] J.C. Snyder, K.A. Thole, Understanding Laser Powder Bed Fusion Surface Roughness, *J. Manuf. Sci. Eng.* (2020), doi:10.1115/1.4046504.
- [158] D.R. Hanson, S.T. McClain, J.C. Snyder, R.F. Kunz, K.A. Thole, Flow in a scaled turbine coolant channel with roughness due to additive manufacturing, in: Proc. ASME Turbo Expo, 2019, doi:10.1115/GT2019-90931.
- [159] A.J. Wildgoose, K.A. Thole, P. Sanders, L. Wang, Impact of Additive Manufacturing on Internal Cooling Channels with Varying Diameters and Build Directions, *ASME Turbo Expo 2020 Turbomach. Tech. Conf. Expo.*, 2020.
- [160] Z. Min, G. Huang, S.N. Parbat, L. Yang, M.K. Chyu, Experimental investigation on additively manufactured transpiration and film cooling structures, *J. Turbomach.* 141 (2019) 1–10, doi:10.1115/1.4042009.
- [161] Z. Min, S.N. Parbat, L. Yang, M.K. Chyu, Thermal-fluid and mechanical investigations of additively manufactured geometries for transpiration cooling, in: Proc. ASME Turbo Expo, 2019, doi:10.1115/GT2019-91583.
- [162] G. Huang, Z. Min, L. Yang, P.X. Jiang, M. Chyu, Transpiration cooling for additive manufactured porous plates with partition walls, *Int. J. Heat Mass Transf.* (2018), doi:10.1016/j.ijheatmasstransfer.2018.03.110.
- [163] L. Yang, Z. Min, S.N. Parbat, M.K. Chyu, Effect of pore blockage on transpiration cooling with additive manufacturable perforate holes, in: Proc. ASME Turbo Expo, 2018, doi:10.1115/GT201875310.
- [164] S.N. Parbat, L. Yang, Z. Min, M.K. Chyu, Experimental and numerical analysis of additively manufactured coupons with parallel channels and inline wall jets, *J. Turbomach.* (2019), doi:10.1115/1.4041821.
- [165] S. Parbat, L. Yang, M. Chyu, S.C. Siw, C.P. Lee, Numerical study of heat transfer in novel wavy trailing edge design for gas turbine airfoils, in: Proc. ASME Turbo Expo, 2019, doi:10.1115/GT2019-91123.
- [166] E. Chia, B.S. Kang, M. Zheng, Y. Li, M. Chyu, Development of ODS coating for high temperature turbine components using DED additive manufacturing, in: Proc. ASME Turbo Expo, 2018, doi:10.1115/GT2018-76274.
- [167] C.U. Gonzalez-Valle, S. Samir, B. Ramos-Alvarado, Experimental investigation of the cooling performance of 3-D printed hybrid water-cooled heat sinks, *Appl. Therm. Eng.* (2020), doi:10.1016/j.applthermaleng.2019.114823.
- [168] Y. Han, B.L. Lau, X. Zhang, Y.C. Leong, K.F. Choo, Thermal Management of Hotspots with a Microjet-Based Hybrid Heat Sink for GaN-on-Si Devices, *IEEE Trans. Components, Packag. Manuf. Technol.* (2014), doi:10.1109/TCPMT.2014.2335203.
- [169] A.J. Robinson, W. Tan, R. Kempers, J. Colenbrander, N. Bushnell, R. Chen, A new hybrid heat sink with impinging micro-jet arrays and microchannels fabricated using high volume additive manufacturing, *Annu. IEEE Semicond. Therm. Meas. Manag. Symp.* 2017, doi:10.1109/SEMI-THERM.2017.7896927.
- [170] R. Kempers, J. Colenbrander, W. Tan, R. Chen, A.J. Robinson, Experimental characterization of a hybrid impinging microjet-microchannel heat sink fabricated using high-volume metal additive manufacturing, *Int. J. Thermofluids*. (2020), doi:10.1016/j.ijft.2020.100029.
- [171] T. Wei, H. Oprins, V. Cherman, S. Yang, I. De Wolf, E. Beyne, M. Baelmans, Experimental Characterization of a Chip-Level 3-D Printed Microjet Liquid Impingement Cooler for High-Performance Systems, *IEEE Trans. Components, Packag. Manuf. Technol.* (2019), doi:10.1109/TCPMT.2019.2905610.
- [172] T.W. Wei, H. Oprins, V. Cherman, I. De Wolf, E. Beyne, S. Yang, M. Baelmans, 3D printed liquid jet impingement cooler: Demonstration, opportunities and challenges, in: Proc. - Electron. Components Technol. Conf., 2018, doi:10.1109/ECTC.2018.00360.
- [173] T.W. Wei, H. Oprins, V. Cherman, I. De Wolf, E. Beyne, M. Baelmans, First demonstration of a low cost/customizable chip level 3D printed microjet hotspot-targeted cooler for high power applications, in: Proc. - Electron. Components Technol. Conf., 2019, doi:10.1109/ECTC.2019.00027.
- [174] B. Kwon, T. Foulkes, T. Yang, N. Miljkovic, W.P. King, Air Jet Impingement Cooling of Electronic Devices Using Additively Manufactured Nozzles, *IEEE Trans. Components, Packag. Manuf. Technol.* 10 (2020) 220–229, doi:10.1109/TCPMT.2019.2936852.
- [175] K.K. Bodla, J.Y. Murthy, S.V. Garimella, Microtomography-based simulation of transport through open-cell metal foams, *Numer. Heat Transf. Part A Appl.* (2010), doi:10.1080/10407782.2010.511987.
- [176] S.T. McClain, D.R. Hanson, E. Cinnamon, J.C. Snyder, R.F. Kunz, K.A. Thole, Flow in a Simulated Turbine Blade Cooling Channel With Spatially Varying Roughness Caused by Additive Manufacturing Orientation, *J. Turbomach.* (2021) 143, doi:10.1115/1.4050389.
- [177] B.V. Ravi, P. Singh, S.V. Ekkad, Numerical investigation of turbulent flow and heat transfer in two-pass ribbed channels, *Int. J. Therm. Sci.* 112 (2017) 31–43, doi:10.1016/j.ijthermalsci.2016.09.034.
- [178] A.K. Viswanathan, D.K. Tafti, Detached eddy simulation of flow and heat transfer in fully developed rotating internal cooling channel with normal ribs, *Int. J. Heat Fluid Flow.* 27 (2006) 351–370, doi:10.1016/j.ijheatfluidflow.2005.12.003.
- [179] J.D. Bernardin, K. Ferguson, D. Sattler, The testing and model validation of an additively manufactured twisted tube heat exchanger, *ASME 2019 Heat Transf. Summer Conf. HT 2019, Collocated with ASME 2019 13th Int. Conf. Energy Sustain.* 2019, doi:10.1115/HT2019-3500.
- [180] C. Busse, H. Freund, W. Schwieger, Intensification of heat transfer in catalytic reactors by additively manufactured periodic open cellular structures (POCS), *Chem. Eng. Process. Process Intensif.* 124 (2018) 199–214, doi:10.1016/j.cep.2018.01.023.
- [181] S. Chekurov, J. Kajaste, K. Saari, H. Kauranen, M. Pietola, J. Partanen, Additively manufactured high-performance counterflow heat exchanger, *Prog. Addit. Manuf.* (2019), doi:10.1007/s40964-018-0059-x.
- [182] E.M. Dede, S.N. Joshi, F. Zhou, Topology Optimization, Additive Layer Manufacturing, and Experimental Testing of an Air-Cooled Heat Sink, *J. Mech. Des. Trans. ASME.* 137 (2015) 1–9, doi:10.1115/1.4030989.
- [183] W.D. Gerstler, D. Erno, Introduction of an additively manufactured multifurcating heat exchanger, in: Proc. 16th Intersoc. Conf. Therm. Thermomechanical Phenom. Electron. Syst. ITherm, 2017, p. 2017, doi:10.1109/ITHERM.2017.7992545.
- [184] D.M. Hyms, M.A. Arle, F. Singer, A.H. Shooshtari, M.M. Ohadi, Enhanced air-side heat transfer in an additively manufactured polymer composite heat exchanger, in: Proc. 16th Intersoc. Conf. Therm. Thermomechanical Phenom. Electron. Syst. ITherm, 2017, p. 2017, doi:10.1109/ITHERM.2017.7992546.
- [185] C. Comotti, D. Regazzoni, C. Rizzi, A. Vitali, Additive manufacturing to advance functional design: An application in the medical field, *J. Comput. Inf. Sci. Eng.* (2017), doi:10.1115/1.4033994.
- [186] M. Javaid, A. Haleem, 3D printed tissue and organ using additive manufacturing: An overview, *Clin. Epidemiol. Glob. Heal.* (2020), doi:10.1016/j.cegh.2019.12.008.
- [187] M.A. Arie, A.H. Shooshtari, R. Tiwari, S.V. Dessiatoun, M.M. Ohadi, J.M. Pearce, Experimental characterization of heat transfer in an additively manufactured polymer heat exchanger, *Appl. Therm. Eng.* 113 (2017) 575–584, doi:10.1016/j.applthermaleng.2016.11.030.
- [188] M. Pelanconi, M. Barbato, S. Zavattoni, G.L. Vignoles, A. Ortona, Thermal design, optimization and additive manufacturing of ceramic regular structures to maximize the radiative heat transfer, *Mater. Des.* 163 (2019) 107539, doi:10.1016/j.matdes.2018.107539.
- [189] D. Singh, W. Yu, D.M. France, T.P. Allred, I.H. Liu, W. Du, B. Barua, M.C. Messner, One piece ceramic heat exchanger for concentrating solar power electric plants, *Renew. Energy.* (2020), doi:10.1016/j.renene.2020.07.070.
- [190] R. Wrobel, B. Scholes, A. Hussein, R. Law, A. Mustaffar, D. Reay, A metal additively manufactured (MAM) heat exchanger for electric motor thermal control on a high-altitude solar aircraft – Experimental characterisation, *Therm. Sci. Eng. Prog.* 19 (2020) 100629, doi:10.1016/j.tsep.2020.100629.
- [191] B.S. Lazarov, O. Sigmund, K.E. Meyer, J. Alexandersen, Experimental validation of additively manufactured optimized shapes for passive cooling, *Appl. Energy.* 226 (2018) 330–339, doi:10.1016/j.apenergy.2018.05.106.
- [192] S. Luque, G. Menéndez, M. Roccabruna, J. González-Aguilar, L. Crema, M. Romero, Exploiting volumetric effects in novel additively manufactured open solar receivers, *Sol. Energy.* 174 (2018) 342–351, doi:10.1016/j.solener.2018.09.030.
- [193] H. Moon, N. Miljkovic, W.P. King, High power density thermal energy storage using additively manufactured heat exchangers and phase change material, *Int. J. Heat Mass Transf.* 153 (2020) 119591, doi:10.1016/j.ijheatmasstransfer.2020.119591.
- [194] A.S. Sabau, A. Bejan, D. Brownell, K. Gluesenkamp, B. Murphy, F. List, K. Carver, C.R. Schairer, J.W. Klett, Design, additive manufacturing, and performance of heat exchanger with a novel flow-path architecture, *Appl. Therm. Eng.* 180 (2020) 115775, doi:10.1016/j.applthermaleng.2020.115775.
- [195] S. Sun, S. Feng, Q. Zhang, T.J. Lu, Forced convection in additively manufactured sandwich-walled cylinders with thermo-mechanical multifunctionality, *Int. J. Heat Mass Transf.* 149 (2020) 1–15, doi:10.1016/j.ijheatmasstransfer.2019.119161.
- [196] A. Takezawa, X. Zhang, M. Kato, M. Kitamura, Method to optimize an additively-manufactured functionally-graded lattice structure for effective liquid cooling, *Addit. Manuf.* 28 (2019) 285–298, doi:10.1016/j.addma.2019.04.004.
- [197] C. Septet, G. El Achkar, O.L. Metayer, J.M. Hugo, Experimental investigation of two-phase liquid-vapor flows in additive manufactured heat exchanger, *Appl. Therm. Eng.* 179 (2020) 115638, doi:10.1016/j.applthermaleng.2020.115638.